ISSN 0915-6364

NATIONAL INSTITUTE FOR FUSION SCIENCE

Cross Sections and Rate Coefficients for Charge Exchange Reactions of Protons with Hydrocarbon Molecules

R.K. Janev, J.G. Wang and T.Kato

(Received - Apr. 16, 2001)

NIFS-DATA-64 May 2001

RESEARCH REPORT
NIFS-DATA Series

TOKI, JAPAN

Cross Sections and Rate Coefficients for Charge Exchange Reactions of Protons with Hydrocarbon Molecules

R. K. Janev[1,2], J. G. Wang[3] and T. Kato[1]

[1] National Institute for Fusion Science, Oroshi-cho,
Toki, Gifu 509-5292, Japan
[2] Macedonian Academy of Sciences and Arts,
P. O. Box 428, 9100 Skopje, Macedonia
[3] Department of Physics and Astronomy, University of Georgia,
Athens, GA 30605, USA

April 21, 2001

Abstract

The available experimental and theoretical cross section data on charge exchange processes in collisions of protons with hydrocarbon molecules have been collected and critically assessed. Using well established scaling relationships for the charge exchange cross sections at low and high collision energies, as well as the known rate coefficients for these reactions in the thermal energy region, a complete cross section database is constructed for proton-C_xH_y charge exchange reactions from thermal energies up to several hundreds keV for all C_xH_y molecules with $x = 1, 2, 3$ and $1 \leq y \leq 2x + 2$. Rate coefficients for these charge exchange reactions have also been calculated in the temperature range from 0.1 eV to 20 keV.

Keywords: electron-molecule collisions, hydrocarbon molecules electron-impact ionization, cross sections, rate coefficients

1. INTRODUCTION

The use of carbon as a plasma facing material (in form of graphite or carbon-carbon composities) in fusion devices is attractive because of its low atomic number that keeps the radiation losses low, and its capability to withstand high heat fluxes without being structurally degraded. For this reason, it has been, and is still being used in many fusion machines, and has been included as one of the plasma facing materials in the divertor design of International Thermonuclear Experimental Reactor (ITER)[1]. However, carbon materials are proved to have extensive chemical erosion when bombarded with hydrogenic particles of energies 50-100 eV and higher. The products of chemical erosion are hydrocarbon molecules, C_xH_y, the composition of which varies with the bombarding energy of hydrogenic particles and surface temperature of carbon materials. At higher particle impact energies (30-500 eV), dominant hydrocarbon species in the erosion fluxes are the light hydrocarbons (CH_3, CH_4, C_2H_2), but with the decrease of impact energy, the heavier hydrocarbon (C_2H_4, C_2H_6, C_3H_4, C_3H_6, C_3H_8) become increasingly more present in the erosion fluxes, and dominant at hyperthermal energies ($\leq 1eV$)[2]. The increase of carbon surface temperature (above 300K) also leads to increase of the presence of heavier hydrocarbons in the erosion fluxes [2]. Most of the presently operating large and medium-size fusion devices (JET, JT-60U, LHD, ASDEX, TEXTOR, Alcator C-mod, DIII-D, etc) have divertors in which the plasma temperature is lowered (by appropriate additional cooling) down to 1-10 eV [3]. Under these conditions, the composition of chemical erosion fluxes is dominated by heavy hydrocarbons C_2H_y, C_3H_y and methane (CH_4).

After their release in the divertor plasma, the hydrocarbon molecules C_xH_y become subject to numerous collision processes with plasma constituents (electrons, protons and neutral hydrogen atoms and molecules). Electron impact excitation and ionization processes of C_xH_y are usually accompanied by molecular fragmentation (dissociation). The recombination of plasma electrons with the $C_xH_y^+$ ions, produced by electron impact ionization and proton charge exchange with C_xH_y, also gives fragmented neutral products (dissociative recombination). Therefore, even if a specific set of CH_y, C_2H_y, C_3H_y hydrocarbon molecules were preferentially formed on the surface and released in the plasma, the above fragmentation collision processes rapidly generate all the members of the CH_y, C_2H_y, C_3H_y families of hydrocarbons.

The cross section database for collision processes of C_xH_y with plasma electrons and protons is still not established, but it is urgently needed to model the transport of eroded carbon in the plasma. Two attempts [4,5] were made in the past to construct such a cross section database. The first of them [4] had a limited scope (containing data only for CH_y, $1 \leq y \leq 4$) and the second [5] was based more on speculative arguments (frequently incorrect) for the cross section relationships between the members of the same family of hydrocarbons, rather than using the available cross section data. Only small part of the cross section data in Ref.4 are based on experimental or theoretical sources; its largest part is also based on speculative arguments and unphysical assumptions.

The present report gives a critical assessment of the available cross section data for charge exchange processes of protons colliding with C_xH_y molecules ($x = 1,2,3; 1 \leq y \leq 2x+2$). Although the cross section data are available for a limited number of C_xH_y molecules, the analysis of their energy behavior allows to identify the electron capture mechanism governing the process in a given energy region and, thereby, to establish (at least approximately) the corresponding cross section scaling law. These scaling laws, together with the known (from the experiment, or Langevin orbiting model) cross sections at thermal collision energies, give a possibility to predict the experimentally unknown cross sections for all the collision system with an accuracy better than factor of two in the range from thermal energies up to about 1 MeV. In the next section we present the charge exchange cross sections for the collision systems for which such data are available either from experimental or theoretical sources. In section 3 we introduce a scaling

form of the experimental cross sections for CH_4, C_2H_6, C_3H_8 and C_4H_{10} based on the revieled electron capture mechanisms for low and high energies. In section 4 we use the cross section scaling properties and other theoretical arguments to construct approximate cross sections for the collision systems for which no data are presently available, and in section 5 we give analytical fits for the recommended cross sections. In section 6, we discuss the charge exchange rate coefficients, while their graphs as functions of plasma temperature and for different values of the "target" energy are given in the Appendix. Finally, in section 7 we give some concluding remarks.

2. THE PROTON CHARGE EXCHANGE CROSS SECTIONS WITH CH_4, C_2H_4, C_2H_6 C_3H_8 and C_4H_{10}

The only C_xH_y molecules for which the proton impact charge exchange cross sections have been measured so far are : CH_4 [6-13], C_2H_2 [13], C_2H_4 [8,9,11],C_2H_6 [9-13], C_3H_8 [10,12,13] and C_4H_{10} [8-10]. Quantum-mechanical cross section calculations have been performed for CH_4 [13,14], C_2H_2 [13,15], C_2H_6 and C_3H_8 [13]. While theoretical calculations cover the region of low collision energies (0.1 - 20 keV), the experimental data cover the energy range from about 0.1 keV up to the MeV region. We note that theoretical calculations in ref.14 (for CH_4) and Ref.15 (for C_2H_2) were done without inclusion of the effects of vibrational excitation of hydrocarbon ionic reaction product and, therefore, they greatly underestimate the corresponding cross sections. The inclusion of these effects in the calculations presented in Ref.13, brings the theoretical cross sections in agreement with experimental data.

We now analyze the cross sections for each of the above $H^+ + C_xH_y$ collision systems separately, excluding the case of $H^+ + C_2H_2$ for which the experimental data are available only in the range 0.2-4.5 keV. (This case will be discussed in Section 4).

2.1 $H^+ + CH_4$

In Fig.1 we present the experimental cross section data for the $H^+ + CH_4$ charge exchange collisions as function of the collision energy taken from Ref. [6-10, 12, 13]. (The data of Ref.11 lie at still higher energies, but are consistent with the high energy trend of the data from Ref.9.) All data are consistent with each other within their experimental errors, except for the high energy points of the earlier experimental results of Koopman [7]. We have plotted in this figure also the recent low-energy data of Kusakabe [16] for the $O^+ + CH_4$ collision system (expressing the collision energy in units of keV/amu), which nicely follow the trend of low-energy data for the $H^+ + CH_4$ system. The basis for this extension of the $H^+ + CH_4$ data with $O^+ + CH_4$ data toward lower energies (down to 0.012 keV/amu) is the equal reaction energy defect for the two collision systems and the fact that the large cross sections (higher than $10^{-15} cm^2$) in this energy region is determined dominantly by the asymptotic forms of the atomic wave functions of initial and final electronic states (i.e. the process takes place at large internuclear distances where the wave function of the active electron is essentially determined by its binding energy). The low-energy behavior of the $H^+ + CH_4$ charge exchange cross section (supplemented with the data for the $O^+ + CH_4$ collision system) indicates that the electron capture process in this energy region (below $\sim$ 20 keV/amu) takes place in a resonant (or almost resonant) manner, i.e. the reaction energy defect is zero (or very close to it). In an initially (energy-) non-resonant but exothermic collision system (the electron binding energies of H and CH_4 are 13.6 eV and 12.6 eV, respectively), the energy resonance condition can occur only if the reaction exothermicity is expended on excitation of the internal degrees of freedom of the reaction fragments. In the case of $H^+ + CH_4$ (or $O^+ + CH_4$) system, the energy resonance condition for the electron capture process is achieved due to the excitation of vibrational and rotational degrees of freedom of the product CH_4^+ ion during the electron transition process. Indeed, the quantum-mechanical molecular-orbital close-coupling (MOCC) calculations performed in Ref.13 for this system could be brought into agreement with the experimen-

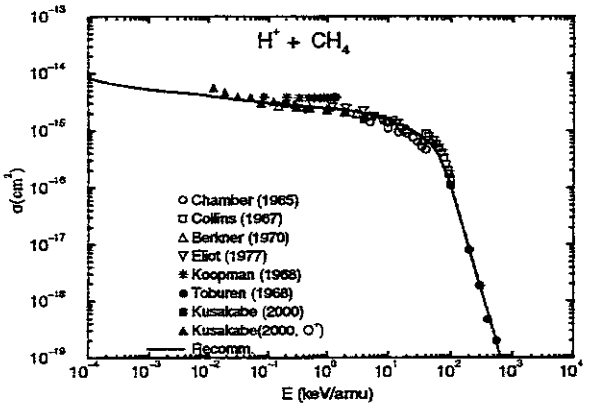

Figure 1: *Total cross sections for the $H^+ + CH_4$ charge exchange collisions as a function of the collisional energy. Symbols represent the experimental data [6-10,12,13,16], and solid curve represents the least square fit of the data (with appropriate extensions;see text).*

tal data of the same reference only with inclusion of vibrationally excited states of CH_4^+ in the calculations.

The revealed resonant character of the electron capture process in the $H^+ + CH_4$ collision system in the low energy region allows us to extend the cross section in the region below the one where experimental data exist (i.e. below 0.01 keV) by using theoretical arguments. The resonant electron capture theory gives the following expression for the low energy charge transfer cross section [17,18]

$$\sigma = A \ln^2(\frac{B}{v}) \qquad (1)$$

where A and B are some constants depending on parameters of colliding system and v is the collision velocity. The validity of this expression is restricted to collision velocities $v \ll 1$, in atomic units, (corresponding to energies $E \ll 25keV/amu$), but greater than some $v = v_{pol}$, below which the electron capture is governed by the Langevin orbiting (or polarization capture) mechanism. The Langevin polarization capture cross section formula can be put in the form [19] (in atomic units)

$$\sigma_L = \frac{2\pi}{v}(\frac{\alpha}{\mu_r})^{1/2} P_\lambda \qquad (2)$$

where α is the polarizability of the molecule, μ_r is the reduced mass of the collision system and P_λ is the probability of decay of the compound, formed by the orbiting mechanism, into the reaction channel λ. For instance, in the $H^+ + CH_4$ collision system, two reaction channels are possible at thermal energies,

$$H^+ + CH_4 \rightarrow (H^+CH_4) \rightarrow H + CH_4^+ \quad (3a)$$
$$\rightarrow H_2 + CH_3^+ \quad (3b)$$

with decay probabilities $P_{3a} \simeq 0.4$ and $P_{3b} \simeq 0.6$. The total thermal rate coefficient, for both channels, is experimentally known [20] and has the value $3.8 \times 10^{-9} cm^3/s$. This value, converted into cross section by the reaction (2), was used to determine the thermal energy limit of the charge exchange cross section for the $H^+ + CH_4$ system in the thermal energy region. The solid curve in Fig.1 represent the best fit of the data and their extension with the $O^+ + CH_4$ data.

2.2. $H^+ + C_2H_4$

The experimental cross section data for the electron capture in $H^+ + C_2H_2$ collision system is available only for energies above 40 keV [8,9,11]. Kusakabe et al. [16] have recently performed electron cross section measurements for the collision system $C^+ + C_2H_4$ in the energy range 0.017-0.38 keV/amu. The charge transfer reaction in this system is exothermic (the ionization potentials of C and C_2H_4 are 11.27 eV and 10.51 eV, respectively) and the data of Kusakabe et. al show that in the energy range where the measurements were performed the cross section for this reaction has a behavior consistent with that for the resonant charge exchange processes. The data are shown in Fig.2. In the thermal energy region (below $\sim$ 0.05 eV), besides the electron capture, there are also two additional exothermic reactions taking place in this collision system

$$H^+ + C_2H_4 \rightarrow (H^+C_2H_4) \rightarrow H + C_2H_4^+ \quad (4a)$$
$$\rightarrow H_2 + C_2H_3^+ \quad (4b)$$
$$\rightarrow H_2 + H + C_2H_2^+ \quad (4c)$$

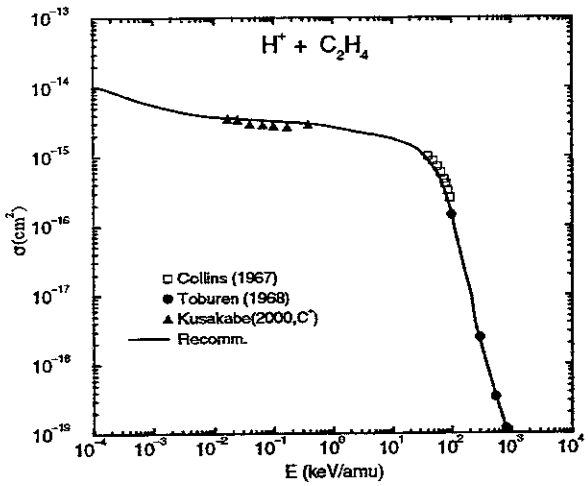

Figure 2: *Total cross sections for the $H^+ + C_2H_4$ charge exchange collisions as a function of the collisional energy. Symbols represent the experimental data [8,9,11,16], and solid curve represents the least square fit of the data (with appropriate extensions;see text).*

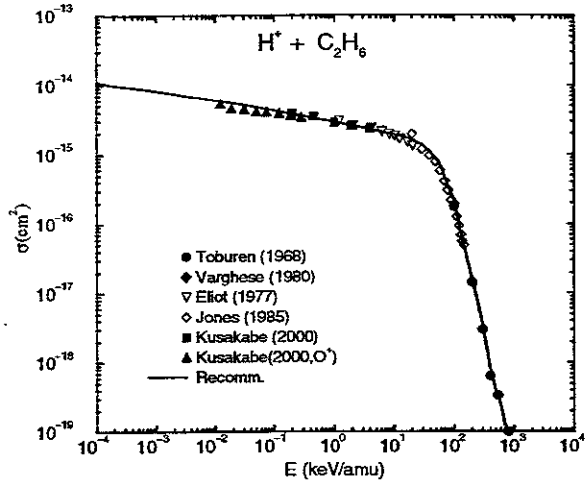

Figure 3: *Total cross sections for the $H^+ + C_2H_6$ charge exchange collisions as a function of the collisional energy. Symbols represent the experimental data [9-13,16], and solid curve represents the least square fit of the data (with appropriate extensions;see text).*

The total rate coefficient for reactions (4a)-(4c), according to Eq.(2), is $K_4 = 4.8\times10^{-9}cm^3/s$, which is distributed among the channels with the probabilities $P_{4a} \simeq 0.3$, $P_{4b} \simeq 0.5$, $P_{4c} \simeq 0.2$. The solid curve in Fig.2 represents the best fit of the available experimental data with an extension towards the thermal energies by taking into account the above value of the Langevin rate coefficients. We note that the decay probability weights for the reactions (4b) and (4c) are determined in accordance with reaction exothermicities.

2.3. $H^+ + C_2H_6$

Experimental cross section data for the electron capture process in $H^+ + C_2H_6$ system are available in the energy range from 0.2 keV up to a few MeV [9-13]. The reaction is exothermic (the ionization potential of C_2H_6 is 11.52 eV) with an energy defect in the initial channel of 2.08 eV. However, this exothermicity can be easily expended on excitation of internal degrees of freedom of $C_2H_6^+$ ion and the cross section data below 20 keV shows a behavior typical for resonant charge exchange (see Fig.3). Moreover, the recent experimental cross section data for the $O^+ + C_2H_6$ system [16] smoothly extend the resonant cross section behavior down to 0.012 keV/amu (also shown in Fig.3). In the thermal energy region (e.g. below $\sim$ 0.05 eV), there are two additional exothermic reactions in the $H^+ + C_2H_6$ system

$$H^+ + C_2H_6 \rightarrow (H^+C_2H_6) \rightarrow H + C_2H_6^+ \quad (5a)$$
$$\rightarrow H_2 + H + C_2H_4^+ \quad (5b)$$
$$\rightarrow H_2 + H_2 + C_2H_3^+ \quad (5c)$$

The reaction channel producing $H_2 + C_2H_5^+$ is endothermic and does not participate in the decay of the complex $(H^+C_2H_6)$. Further, the ion $C_2H_6^+$ has a dissociation energy of about 1 eV with respect to dissociation into $C_2H_4^+ + H_2$ products and can rapidly predissociate into this channel. Therefore, the channels (5a) and (5b) are sometimes treated jointly in the thermal energy region. The total rate coefficient for all the channels (5) is $K_5 = 4.2 \times 10^{-9}cm^3/s$ [21], with channel probabilties $P_{5a} \simeq 0.3$, $P_{5b} \simeq 0.3$ and $P_{5c} \simeq 0.4$. The solid curve in Fig.3 represents a least square fit to the data with an extension towards lower energies consistent with the above rate coefficient value.

2.4 $H^+ + C_3H_8$

Experimental cross section data for the electron capture reaction in this collision system are available in the energy range 0.2-200 keV [10,12,13]. Similar data have recently become available also for the $O^+ + C_3H_8$ system in the energy range 0.012-0.28 keV/amu [16]. The H^+ and O^+ impact data are plotted in Fig.4 and they all show a consistent low energy behavior of the cross section, confirming the resonant character of the process in the region below ~ 20 keV/amu. (The ionization potential of C_3H_8 is 11.08 eV.) In the thermal energy region, the charge exchange is accompanied also by atom exchange, i.e.,

$$H^+ + C_3H_8 \rightarrow (H^+C_3H_8) \rightarrow H + C_3H_8^+ \quad (6a)$$
$$\rightarrow H_2 + C_3H_7^+ \quad (6b)$$

with total rate coefficient $K_6 = 5.2 \times 10^{-9} cm^3/s$ [21], and decay channel probabilities $P_{6a} \simeq P_{6b} \simeq 0.5$. The solid curve in Fig.4 is a fit of the data with an extension towards lower energies consistent with the above value of the rate coefficient. In the region above 200 keV/amu, the cross section is derived by using the scaling relation discussed in Section 3.

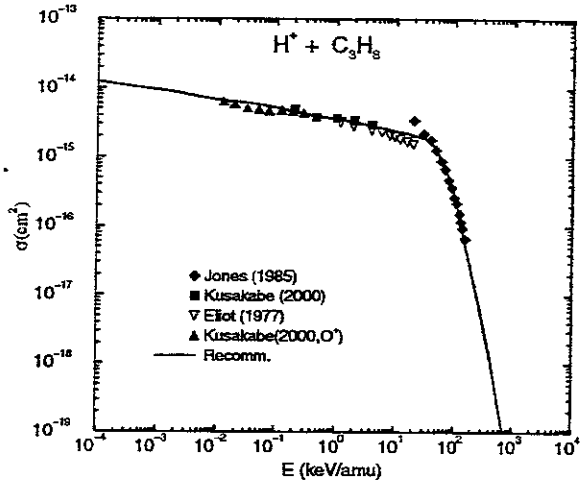

Figure 4: *Total cross sections for the $H^+ + C_3H_8$ charge exchange collisions as a function of the collisional energy. Symbols represent the experimental data [10,12,13,16], and solid curve represents the least square fit of the data (with appropriate extensions;see text).*

2.5. $H^+ + C_4H_{10}$

The electron capture cross section data for this collision system are available only in the region above 1 keV (up to 1 MeV) [8-10] and are shown in Fig.5. The low-energy data (below $\sim$ 20 keV) indicate that this reaction also has a resonant character, consistent with its high exothermicity (the ionization potential of C_4H_{10} is 10.53 eV) and the large number of vibrational modes of $C_4H_{10}^+$ product ion (available to absorb the reaction exothermicity during the capture process and provide resonance conditions for the process). Since the rate coefficient for this reaction in the thermal energy region is unknown, we have calculated it by using the relation

$$K_{10} \simeq K_8 (\frac{\alpha_{10}}{\alpha_8})^{1/2} \quad (7)$$

following from Eq.(2), where the subscripts "8" and "10" refer to the C_3H_8 and C_4H_{10} molecules, the polarizabilities of which are known: $\alpha_8 = 42.49$, $\alpha_{10} \simeq 54.7$, in atomic units (a_o^3)[22]. This gives the value for K_{10} of $5.9 \times 10^{-9} cm^3/s$. The solid curve in Fig.5 is a fit to the experimental data, extended towards the low energies in accordance with the above value for K_{10}.

At the end of this section we would like to make the following remark. It can be observed that the high energy dependence of the cross sections for the considered collision system somewhat changes (the cross section curves change their slope) at the energies above 400 - 500 keV (see Figs.1-3,5). The observed increase of the cross sections in this energy region is due to the contribution to the process of electron capture from the inner shells of C_xH_y.

3. CROSS SECTION SCALING RELATIONS

The similarity in the cross section energy behavior for all $H^+ + C_xH_y$ collision systems considered in the preceding section indicates that the electron capture process in these systems is governed by the same physical mechanism at low energies ($E \leq 20keV$) and another physical mech-

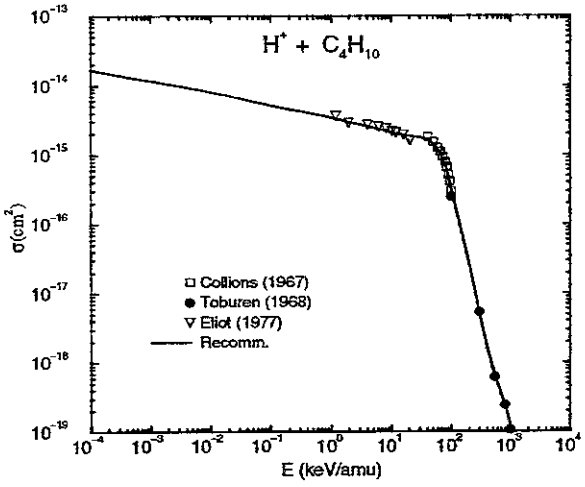

Figure 5: *Total cross sections for the $H^+ + C_4H_{10}$ charge exchange collisions as a function of the collisional energy. Symbols represent the experimental data [8-10], and solid curve represents the least square fit of the data (with appropriate extensions;see text).*

anism (but same for all collision systems) at the high energies (above $\sim 100keV$). We have already argued that the low-energy transition mechanism is the resonant capture mechanism, characterized by a cross section energy behavior in the form of Eq.(1). From the theory of resonant charge exchange reactions (see e.g. [17],[18]), it follows that the constant A in Eq.(1) is proportional to $1/I_p$, where I_p is the ionization potential of the molecule. The constant B in Eq.(1) is proportional to the number of equivalent electrons in the target, which we take to be equal to the number y of H-atoms in the C_xH_y molecule. For $4 \leq y \leq 8$, $ln^2 y$ can be approximated by $y^{1/2}$ to within an accuracy of 37%, or better. Therefore, in the low energy region, the resonant capture cross section can be approximately represented in a reduced form

$$\overline{\sigma}_l = \sigma I_p / y^{1/2}. \qquad (8)$$

In the energy region above $\sim 100keV$, most of the theoretical models (e.g. the classical impulse approximation, the first Born approximation, etc) show an I_p^{-2} dependence of the charge exchange cross section (see e.g. [23]). Assuming that the electron donors of the C_xH_y molecule in the electron capture process, are the H atoms, and that at high energies these atoms can be considered as independent donors, it follows that the cross sections at these energies is proportional to the numbers y of H atoms in the C_xH_y molecule. Therefore, in the region above 100-200 keV, the approximate reduced form of charge exchange cross section is

$$\overline{\sigma}_h = \frac{\sigma I_P^2}{y} \qquad (9)$$

In the intermediate energy range ($\sim 20 - 100keV$), the electron capture process in any ion-atom or ion-molecule collision system results from the coupling of many electronic states and no simple dependence of σ on I_p and y can be theoretically predicted. For the practical purpose of constructing a reduced cross section $\overline{\sigma}$ in the entire energy region, one can bridge these interval by taking the average value of $\overline{\sigma}_l$ and $\overline{\sigma}_h$,

$$\overline{\sigma}_m = (\overline{\sigma}_l + \overline{\sigma}_h)/2 \qquad (10)$$

Using the scaling relations (8)-(10), we have plotted the experimental data for CH_4 , C_2H_6, C_3H_8 and C_4H_{10} in Fig.6 in a reduced form, $\overline{\sigma}(E)$. The scaled data show a pronounced tendency of grouping around a single curve, their dispersion being result of the approximate character of the scalings (8)-(10), but also a reflection of the experimental uncertainties of the original data. The solid line in Fig.6 represents a best-square fit of the data. The extension of this line towards lower collision energy was done by using the scaled fits of the cross section for these systems in the energy region below 1eV. It should be noted that the scaling relation (8) is valid only for those systems for which the electron capture process has a resonance character. We could expect that the energy resonance conditions for the processes can be met for the C_xH_y molecules with sufficiently large number of H atoms (e.g. $y \geq 2x$, or so). The high energy scaling relation (9), however, should be valid for any C_xH_y molecule.

4. DERIVED CROSS SECTIONS FOR OTHER $H^+ + C_XH_Y$ SYSTEM

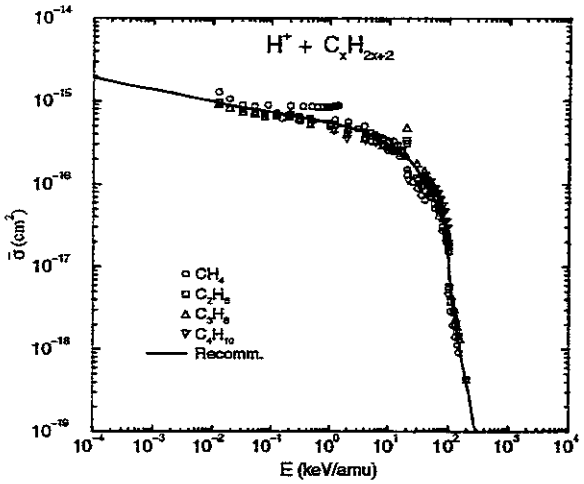

Figure 6: *Total cross sections in a reduced form (Eqs.(8)-(10)) for the CH_4, C_2H_6, C_3H_8 and C_4H_{10} charge exchange collisions as a function of the collisional energy. Symbols represent the experimental data [6-13,16], and solid curve represents the least square fit of the data, extended to scaled thermal-energy cross section values.*

In order to perform a complete modeling of the transport of hydrocarbons in a plasma one needs to know the cross sections (or rate coefficients) for all members of the hydrocarbon families C_xH_y, for x=1-3 and $1 \leq y \leq 2x+2$, and for all important processes. Charge exchange is certainly one of those processes, especially for the temperatures characterizing the edge and divertor plasmas. (The C_4H_{10} family of hydrocarbons will be excluded from our further considerations.) Since apart from the systems discussed in Section 2, experimental (and theoretical) information exists only for the $H^+ + C_2H_2$ system (but only in the energy range 0.2-4.5 keV [15]), one is left with the necessity to derive approximate cross sections for the remaining $H^+ + C_xH_y$ collision systems on the basis of the scaling laws discussed in the previous section, the information about the thermal rate coefficients available from Ref.21, and by using the general theory of charge exchange reactions [18,23,24]. In deriving the approximate cross sections for the systems for which data are not available (above the thermal energy region) from the literature, it is convenient to separate the $H^+ + C_xH_y$ collision systems into two classes: systems in which the process has resonant character and systems with non-resonant electron capture. This separation is mainly applicable for the low energy region, since at high energies the electron transition mechanism is less sensitive to the energy resonance condition [23,24]. The criteria for the expected fulfillment of the resonant energy condition for the charge exchange process in $H^+ + C_xH_y$ systems were discussed at the end of the preceding section. We should note that the "resonant electron capture" is used here in a broader sense (equality or near equality of the total internal energy in the initial and final reaction states) and is not related to the symmetry properties of the collision system (like in the case of resonant electron capture in isonuclear atomic and molecular collision systems).

4.1 Resonant $H^+ + C_xH_y$ Charge Exchange Reactions

We have seen in Section 2 that the charge exchange reactions in $H^+ + CH_4$, C_2H_4,C_2H_6, C_3H_8 collision systems have a resonant character in the low energy region. In the next subsection, we shall see that the experimental cross section data for the $H^+ + C_2H_2$ reaction in the energy range 0.2-4.5 keV show a behavior departing (but not drastically) from the resonant cross section behavior. This can be taken as an indication that for the $H^+ + C_xH_y$ with $x = 2, 3$ and $y \geq 2x - 1$ the process attains its resonant character. Therefore, for these systems, as well as for CH_3, the cross section above the thermal energy region can be derived from the cross section for C_xH_{2x+2} (given in Section 2) by using the scaling relations (8)-(10). Below $\sim$ 0.5 eV, these cross sections should be extended in such a way as to smoothly go over into the values determined by the known reaction rate coefficients [21]. In Table I we give the total rate coefficients for all $H^+ + C_xH_y$ reactions [21], together with the branching ratios (probabilities P_λ) for the different channels of the orbiting compound decay. We note that not in all cases we have used the branching ratios adopted in Ref.21, but rather we have taken into account the trend of

the charge exchange cross section behavior as suggested by the recent low-energy experimental data [15,16], (not available in the time when Ref.21 was published), as well as the values of exothermicities of the particular reaction channels. We further note that in Ref.5, the total rate coefficient for (H^+,C_xH_y) compound formation, $\sigma_l v = K_L$ was calculated by using the Langevin formula (Eq.(2) with $P_\lambda = 1$)) and then assigning equal branching ratios to all reaction channels. The assignment of equal decay probability P_λ to all reaction channels in Ref.5 leads to significant uncertainties in the derived cross sections.

A further remarks is noteworthy here regarding the energy dependence of the channel cross sections in the thermal energy reactions

$$\begin{aligned} H^+ + C_xH_y &\rightarrow (H^+C_xH_y) \\ &\rightarrow H + C_xH_y^+ \qquad (11a) \\ &\rightarrow H_2 + C_xH_{y-1}^+ \qquad (11b) \\ &\rightarrow H_2 + H + C_xH_{y-2}^+ \qquad (11c) \\ &\rightarrow H_2 + H_2 + C_xH_{y-3}^+ \qquad (11d) \\ &\quad ..... \end{aligned}$$

While the $1/v$ dependence is common to the cross sections of all the channels of reaction (11) in the thermal energy region (e.g. below $\sim$ 0.05 eV), the decrease of the cross section with increasing the collision energy is much faster for the particle exchange and break-up channels (11b)-(11d) than for the electron transfer channel (11a), which continues to follow the $1/v$ dependence in a much larger energy region. These different energy dependences of the cross sections for the reaction channels (11a) and (11b)-(11d) have to be taken into account when trying to smoothly connect the cross sections from the resonant region (when experimental electron capture data for the $H^+ + C_xH_{2x+2}$ exist) with the cross section for the channel (11a). If $K_\lambda = K_{tot}P_\lambda$ is the thermal rate coefficient for the reaction channel λ in Eq.(11), and K_{tot} is the total thermal rate coefficient for all channels, expressed in units of cm^3/s, then the thermal energy cross sections of the channel (11a) and channels (11b)-(11d) can be expressed as

$$\sigma_{11a} = 7.26 \times 10^{-7} \frac{K_{11a}(cm^3/s)}{E(eV)^{1/2}} (cm^2) \quad (12)$$

$$\begin{aligned} \sigma_\lambda &= 7.26 \times 10^{-7} \frac{K_\lambda(cm^3/s)}{E(eV)^{1/2} + aE(eV)^\beta} (cm^2), \\ &\lambda = (11b) - (11d), \qquad (13) \end{aligned}$$

where a (< 1) and β (> 1) are constants given in Table I for each of the reaction channels.

The scaling relations (8)-(10) were used for deriving the resonant cross sections for the systems $H^+ + C_xH_y$, $y \geq 2x - 1$ separately for each of the C_xH_y families of hydrocarbons. For instance, the cross sections for the $H^+ + C_3H_y$, $5 \leq y \leq 7$, collision system were derived by relating the cross section for each of them with the cross section for the system $H^+ + C_3H_8$ by using Eqs.(8)-(10). The ionization potentials I_p of the C_xH_y molecules, needed in the use of Eqs.(8)-(10) are given in Table II. These data were collected from the literature, or calculated from the thermochemical tables [25,26].

The cross sections for the resonant $H^+ + C_xH_y$ ($2x - 1 \leq y \leq 2x + 2$) charge exchange reactions are given in Fig.7 (for CH_y), Fig.8 (for C_2H_y) and Fig.9(for C_3H_y), together with the cross sections for the non-resonant reactions.

It should be noted that the cross sections for the system $H^+ + C_xH_{2x+1}$ in the low-energy region are larger than the cross sections for the $H^+ + C_xH_{2x+2}$ systems, which is a consequence of the scaling relation (8) and the fact that the ionization potentials of C_xH_{2x+1} are smaller than those for C_xH_{2x+2} (see Table II).

4.2 Non-resonant $H^+ + C_xH_y$ Charge Exchange Reactions

The only non-resonant charge exchange reaction in the $H^+ + C_xH_y$ collision systems for which the cross section has been measured in the energy range 0.2-4.5 keV is the reaction $H^+ + C_2H_2$ [13]. There have been recently cross section measurement also for the charge exchange reaction $O^+ + C_2H_2$ in the energy range 0.012-0.3 keV/amu.

TABLE I: TOTAL THERMAL RATE COEFFICIENTS, BRANCHING RATIOS AND VALUES OF PARAMETERS α AND β IN EQ.(13) FOR THE $H^+ + C_xH_y$ CHARGE EXCHANGE REACTIONS

Reaction	Branching Ratios,P_λ	Total Rate Coef.($10^{-9}cm^3/s$)	α	β
$H^+ + CH_4 \rightarrow H + CH_4^+$	0.4	3.8	-	-
$\rightarrow H_2 + CH_3^+$	0.6		0.5	2.5
$H^+ + CH_3 \rightarrow H + CH_3^+$	1.0	3.4	-	-
$H^+ + CH_2 \rightarrow H + CH_2^+$	0.36	2.8	-	-
$\rightarrow H_2 + CH^+$	0.64		0.5	2.5
$H^+ + CH \rightarrow H + CH^+$	0.31	1.9	-	-
$\rightarrow H_2 + C^+$	0.69		0.01	3.5
$H^+ + C_2H_6 \rightarrow H + C_2H_6^+$	0.29	4.2	-	-
$\rightarrow H + H_2 + C_2H_4^+$	0.33		0.45	2.5
$\rightarrow H_2 + H_2 + CH_3^+$	0.38		0.45	2.5
$H^+ + C_2H_5 \rightarrow H + C_2H_5^+$	0.40	4.5	-	-
$\rightarrow H_2 + C_2H_4^+$	0.49		0.45	2.5
$\rightarrow H + H_2 + C_2H_3^+$	0.11		0.45	2.5
$H^+ + C_2H_4 \rightarrow H + C_2H_4^+$	0.31	4.8	-	-
$\rightarrow H_2 + C_2H_3^+$	0.52		0.45	2.5
$\rightarrow H + H_2 + C_2H_2^+$	0.17		0.45	2.5
$H^+ + C_2H_3 \rightarrow H + C_2H_3^+$	0.77	4.0	-	-
$\rightarrow H_2 + C_2H_2^+$	0.23		0.5	2.5
$H^+ + C_2H_2 \rightarrow H + C_2H_2^+$	0.71	3.5	-	-
$\rightarrow H_2 + C_2H^+$	0.29		0.45	2.5
$H^+ + C_2H \rightarrow H + C_2H^+$	0.5	3.0	-	-
$\rightarrow H_2 + C_2^+$	0.5		0.45	2.5
$H^+ + C_3H_8 \rightarrow H + C_3H_8^+$	0.5	5.2	-	-
$\rightarrow H_2 + C_3H_7^+$	0.5		0.6	3.0
$H^+ + C_3H_7 \rightarrow H + C_3H_7^+$	0.5	5.0	-	-
$\rightarrow H_2 + C_3H_6^+$	0.5		0.6	3.0
$H^+ + C_3H_6 \rightarrow H + C_3H_6^+$	0.5	4.8	-	-
$\rightarrow H_2 + C_3H_5^+$	0.5		0.6	3.0
$H^+ + C_3H_5 \rightarrow H + C_3H_5^+$	0.5	4.6	-	-
$\rightarrow H_2 + C_3H_4^+$	0.5		0.6	3.0
$H^+ + C_3H_4 \rightarrow H + C_3H_4^+$	0.5	4.4	-	-
$\rightarrow H_2 + C_3H_3^+$	0.5		0.6	3.0
$H^+ + C_3H_3 \rightarrow H + C_3H_3^+$	0.5	4.2	-	-
$\rightarrow H_2 + C_3H_2^+$	0.5		0.8	3.0
$H^+ + C_3H_2 \rightarrow H + C_3H_2^+$	0.5	4.0	-	-
$\rightarrow H_2 + C_3H^+$	0.5		1.0	3.0
$H^+ + C_3H \rightarrow H + C_3H^+$	0.5	4.0	-	-
$\rightarrow H_2 + C_3^+$	0.5		1.6	3.0

TABLE II: IONIZATION POTENTIALS OF C_xH_y

C_xH_y	$I_p(eV)$	C_xH_y	$I_p(eV)$
CH_4	12.51	C_3H_8	11.08
CH_3	9.84	C_3H_7	9.10
CH_2	10.46	C_3H_6	9.74
CH	11.13	C_3H_5	9.90
C_2H_6	11.52	C_3H_4	10.02_{av}
C_2H_5	8.25	(Propyne)	10.36
C_2H_4	10.51	(Allene)	9.69
C_2H_3	9.45	C_3H_3	8.34
C_2H_2	11.51	C_3H_2	12.50
C_2H	17.42	C_3H	13.40

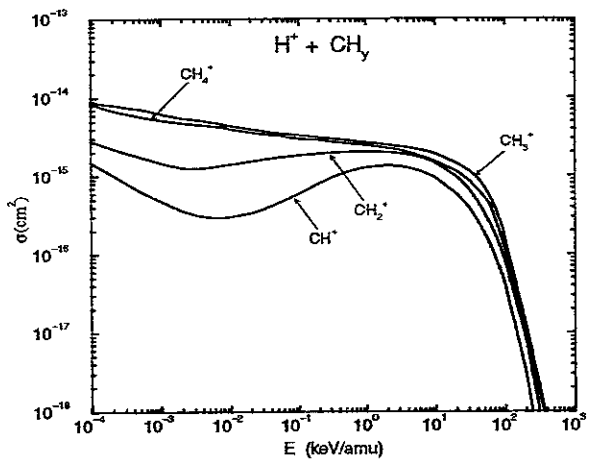

Figure 7: *Cross sections for the* $H^+ + CH_y(y = 1-4)$ *charge exchange collisions as a function of the collisional energy.*

These data are shown in Fig.10 and they follow a single line. The solid line through the data represents their fit. This line is smoothly continued towards the low energies in such a way that it goes over into the thermal energy electron capture cross section of the form of Eq.(12) with the value of rate coefficients (K_{11a}) given in Table I.

In the energy region above $\sim 20keV$, the cross section has been determined by using the scaling relations (9) and (10) in conjunction with the known cross section data for the $H^+ + C_2H_4$ and $H^+ + C_2H_6$ reactions. Since the experimental data above 3 eV show already a very slow increase (see Fig.10), a smooth connection of the

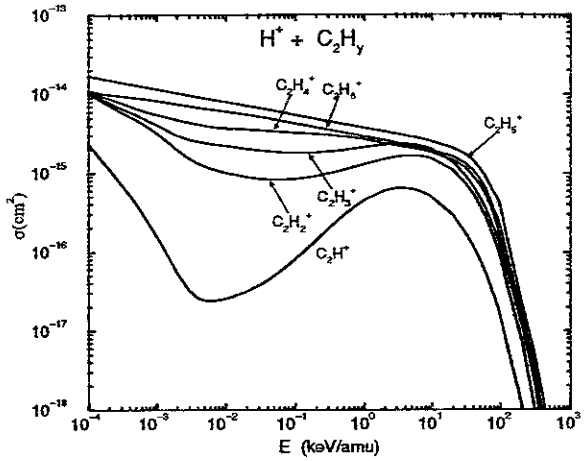

Figure 8: *Cross sections for the* $H^+ + C_2H_y(y = 1-6)$ *charge exchange collisions as a function of the collisional energy.*

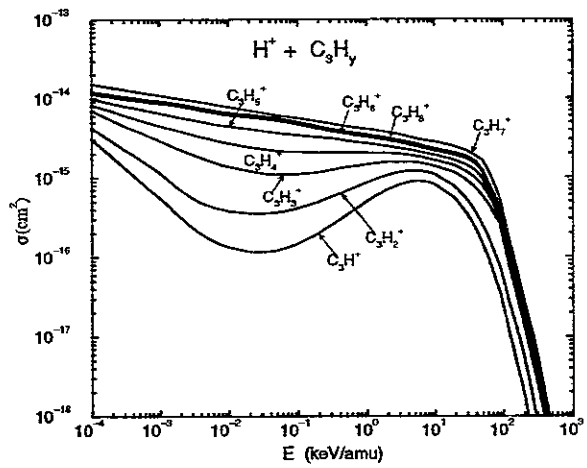

Figure 9: *Cross sections for the* $H^+ + CH_y(y = 1-8)$ *charge exchange collisions as a function of the collisional energy.*

data below 4.5 keV with those above 20 keV is possible using the fact that the velocity at which the cross section maximum occurs is given by the Massey relation (in atomic units)

$$c\Delta E/v \simeq 1 \qquad (14)$$

where v is the collision velocity, $\Delta E = I_P(H) - I_P(C_2H_2) = 2.2eV$, and c is some constant. The cross section maximum at ~ 10 keV for the $H^+ + C_2H_2$ reaction gives the value of $c \simeq 8$. This value of c will be taken as typical also for the other non-resonant $H^+ + C_xH_y$ charge exchange reactions. The relations (14) shows that for reactions with larger ΔE, the cross section maximum appears at larger energies.

The non-resonant charge exchange reaction in ion-atom/molecule collision systems are generally described by Demkov's (two state) model [18] which predicts a rapid decrease of the cross section when the energy decreases below the value at which the cross section maximum occurs. This decrease is faster (exponential) for the reactions with larger energy defect. However, if the polarizability of the neutral reactant is high, like in the case of hydrocarbon molecules (for CH_4, C_2H_6 and C_3H_8 the values of α are 17.56, 30.20 and 42.5 a_o^3, respectively[22]), the mechanism of polarizational capture (Langevin orbiting) starts to operate at larger collision energies and the cross sections starts to increase with decreasing the energy.

In deriving the cross sections for the non-resonant $H^+ + C_xH_y$ charge exchange (other than for C_2H_2), we have used the scalings (9)-(10) for the energies down to ~ 20 keV, Demkov's model [18] for the energies below $\sim$ 20 keV and the polarization capture model, Eq.(12), for the energies below $\sim$ 1 eV. Since the parameters entering in Demkov's model (e.g. the exchange interaction) are not well known for the considered collision systems, and since the Franck-Condon $C_xH_y \rightarrow C_xH_y^+$ transition factors enter the theory in different ways at the higher ($\sim$ 10 keV) and lower ($\sim 1 - 10$ eV) energies (frozen vs. relaxed vibrational motion), the use of Demkov's model was done in a qualitative manner only (to determine the slope of the cross section decrease

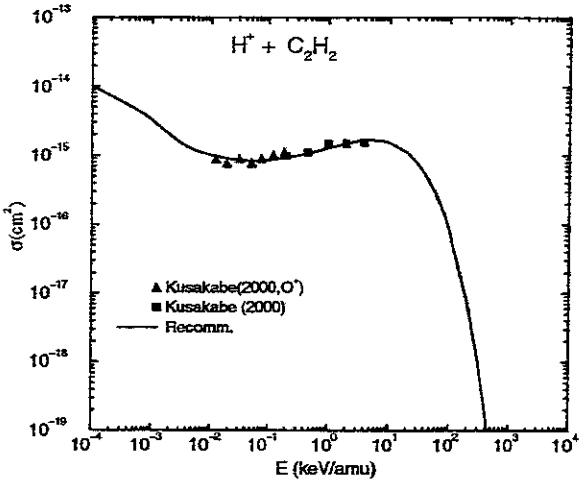

Figure 10: *Total cross sections for the $H^+ + C_2H_2$ charge exchange collisions as a function of the collisional energy. Symbols represent the experimental data [13,16], and solid curve represents the least square fit of the data (with appropriate extensions;see text).*

in the region below the energy of the cross section maximum). Therefore, the cross sections for the $H^+ + C_xH_y$ systems, with $x = 1 - 3$ and $y = 1, 2$ (except for C_2H_2) have large uncertainties in the energy range 1 eV - 10 keV. The cross sections for the non-resonant reactions derived by the procedures described above are shown in Fig.7 (for CH_y), Fig.8 (for C_2H_y) and Fig.9 (for C_3H_y), together with the cross sections of resonant reactions.

5. ANALITIC FITS TO THE CROSS SECTIONS

For an easy incorporation of the present cross sections into various plasma application codes, we have fitted the charge exchange cross section data to the following analytic expression

$$ln(\sigma) = \sum_{i=1}^{N} C_i T_i(x) \qquad (15)$$

where, $x = [(lnE - lnE_{min}) - (lnE_{max} - lnE)] / [lnE_{max} - lnE_{min}]$, E is the collision energy expresses in units of keV, C_i are the fitting coefficients, the units of σ are $10^{-16} cm^2$, and $T_i(x)$ are the Chebyshev orthogonal polynomials ($T_1(x) =$

TABLE III: VALUES OF PARAMETERS C_i IN EQ.(15) FOR THE $H^+ + C_xH_y$ COLLISION SYSTEMS AND THEIR REDUCED FORM EQS.(8)-(10). (The r.m.s. deviation of the fits is shown in the bottom line)

	CH_4	CH_3	CH_2	CH	C_2H_6
C_1	3.901564E-1	6.854778E-1	1.118652E-1	-1.060468E+0	1.275456E+0
C_2	-6.426675E+0	-5.810741E+0	-5.216803E+0	-5.662572E+0	-5.408443E+0
C_3	-3.706893E+0	-3.622136E+0	-3.893841E+0	-4.376450E+0	-3.426843E+0
C_4	-1.999034E+0	-2.179920E+0	-2.756865E+0	-3.567226E+0	-2.298691E+0
C_5	-5.625439E-1	-7.801006E-1	-1.192043E+0	-1.433069E+0	-1.310537E+0
C_6	2.279431E-1	-2.421371E-2	-5.200059E-1	-5.789399E-1	-5.555345E-1
C_7	3.443980E-1	2.762333E-1	-1.816781E-1	-3.523295E-1	-1.044490E-1
C_8	1.566892E-1	2.288237E-1	1.129866E-2	-9.956988E-2	5.031086E-2
C_9	-5.398410E-2	6.164797E-2	-3.658702E-3	1.532751E-2	6.306925E-2
C_{10}	-1.822252E-1				-6.864191E-3
C_{11}	-1.593352E-1				
C_{12}	-8.826322E-2				
Deviation	6%	6%	5%	2%	5%

TABLE III: (continued)

	C_2H_5	C_2H_4	C_2H_3	C_2H_2	C_2H
C_1	1.716499E+00	8.341737E-1	8.888440E-1	2.513870E-1	-1.986507E+0
C_2	-5.230512E+00	-5.821612E+0	-5.243715E+0	-5.812705E+0	-5.720283E+0
C_3	-3.170772E+00	-3.769920E+0	-3.110835E+0	-3.338185E+0	-3.535139E+0
C_4	-2.185277E+00	-2.790407E+0	-2.531330E+0	-3.071630E+0	-4.230273E+0
C_5	-1.232087E+00	-1.480843E+0	-1.113044E+0	-1.433263E+0	-1.254502E+0
C_6	-5.036952E-01	-6.962345E-1	-3.147011E-1	-3.583544E-1	-2.056898E-1
C_7	-7.229334E-02	-2.496726E-1	-5.834419E-2	-1.456216E-1	-4.595756E-1
C_8	8.230586E-02	-8.972341E-3	2.432579E-2	-7.391778E-3	-7.842824E-2
C_9	8.365203E-02	2.066349E-2	-9.508213E-3	1.151712E-2	3.002537E-2
C_{10}	1.283200E-02				-5.626713E-2
C_{11}					6.455583E-2
Deviation	4%	4%	3%	3%	5%

TABLE III: (continued)

	C_3H_8	C_3H_7	C_3H_6	C_3H_5	C_3H_4
C_1	1.403347E+0	1.732713E+0	1.487291E+0	1.239651E+0	9.386948E-01
C_2	-5.455461E+0	-5.142546E+0	-5.211636E+0	-5.153170E+0	-5.123019E+00
C_3	-3.554360E+0	-3.263284E+0	-3.372781E+0	-3.302519E+0	-3.226687E+00
C_4	-2.464602E+0	-2.274484E+0	-2.304268E+0	-2.360416E+0	-2.473107E+00
C_5	-1.438525E+0	-1.321468E+0	-1.360992E+0	-1.335779E+0	-1.322435E+00
C_6	-6.514340E-1	-5.792384E-1	-6.362773E-1	-5.991178E-1	-5.319703E-01
C_7	-1.712580E-1	-1.275364E-1	-1.832337E-1	-1.796747E-1	-1.598061E-01
C_8	1.920722E-3	3.649298E-2	-2.945122E-2	-3.727936E-2	-5.410573E-02
C_9	1.586834E-2	6.265064E-2	5.310641E-3	1.001740E-2	-5.656260E-03
C_{10}	-4.835895E-2	-1.079800E-2	-8.896402E-2	-7.613230E-2	-7.050675E-02
Deviation	2%	2%	6%	8%	7%

TABLE III: (continued)

	C_3H_3	C_3H_2	C_3H	C_4H_{10}	Reduced $\overline{\sigma}$
C_1	6.955227E-1	-2.638408E-1	-1.152102E+0	2.083786E+0	-4.977547E-1
C_2	-4.904809E+0	-5.204029E+0	-5.658128E+0	-4.479109E+0	-5.282566E+0
C_3	-2.961972E+0	-3.135821E+0	-3.394316E+0	-2.435900E+0	-3.084821E+0
C_4	-2.610593E+0	-3.021844E+0	-3.551017E+0	-1.560149E+0	-1.686825E+0
C_5	-1.346304E+0	-1.220869E+0	-1.368680E+0	-7.565884E-1	-5.026824E-1
C_6	-5.076411E-1	-2.175365E-1	-1.457613E-1	-1.216295E-1	2.047167E-1
C_7	-2.245476E-1	-1.076868E-1	-7.089518E-2	2.540721E-1	4.754529E-1
C_8	-9.378583E-2	-9.698729E-3	-4.108061E-2	3.300761E-1	3.703372E-1
C_9	-2.851315E-2	8.886834E-3	8.174401E-3	2.530929E-1	2.414728E-1
C_{10}				9.383315E-2	
Deviation	8%	8%	7%	7%	8%

1, $T_2(x) = x$, and $T_{n+2}(x) = 2T_{n+1}(x) - T_n(x)$). For all the reactions considered, the $E_{min} = 10^{-4}$ keV and $E_{max} = 10^3$ keV, and the fitting coefficients C_i are given in Table III. The r.m.s. deviation of the fits from the cross section values that have been fitted is somewhat different for different reactions and is in the range $2\% - 8\%$. (The r.m.s. value for each reaction is also shown in Table III).

The solid curve on Fig.6, which represent the fit to the experimental data for the $H^+ + CH_4$, C_2H_6, C_3H_8 and C_4H_{10} systems, can also be represented by the same expression as the Eq.(15). This reduced cross section, which represents the data with an accuracy of about $20 - 30\%$ in the low energy region, and with an accuracy of $30 - 40\%$ in the high energy region, can also be used to derive the cross sections for other $H^+ + C_xH_y$ resonant reactions.

6. REACTION RATE COEFFICIENTS

The rate coefficient $< \sigma v >$ of a heavy particle reaction (like charge exchange) between a particle of mass m and fixed energy $E_i = mV^2/2$ incident on a Maxwellian distribution of particles of mass M and temperature $T = Mu^2/2$ is given by [27]

$$< \sigma v > = \frac{4}{\pi^{1/2} u V} \int_{v_{th}}^{\infty} v_r^2 dv_r \sigma(E_r) \{exp[-(v_r - V)^2/u^2] - exp[-(v_r + V)^2/u^2]\} \quad (16)$$

where $v_r = |\vec{V} - \vec{u}|$ is the relative (collision) velocity related to E_r by $E_r = m_r v_r^2/2$, $m_r = mM/(m+M)$ being the reduced mass of colliding particles, and v_{th} is the value of v_r at the threshold, $E_r = E_{th}$. All charge excharge reactions covered by the present report are exothermic and for all of them $E_{th} = 0$.

We have calculated the rate coefficients for the considered $H^+ + C_xH_y$ charge exchange reactions by using Eq. (16) for five values of parameter E_i, E_i=0.1,1,10,100 and 1000 eV in the temperature range T=0.1-20 keV. The analytical cross section fits for σ, Eq.(15), where used in these calculations. The results are shown in the Graphs 1-18 in the Appendix. The thick solid line on each of the graphs represents the recommended cross section of the corresponding reaction in the energy range E=0.1 eV-20 keV, for which the right-hand side ordinate of the graph applies. We note that the rates for the $H^+ + CH_y$ charge exchange reactions, calculated with the cross sections of the present report are drastically different from those given in Ref. [4]. In fact, in Ref. [4] the cross section for the $H^+ + CH_4$ reaction was assigned to all other $H^+ + CH_y (1 \leq y \leq 3)$ collision systems, producing the same rates for all of them.

7. CONCLUDING REMARKS

We have compiled and assessed the existing experimental cross section data for the charge exchange process in $H^+ + C_xH_y$ collision systems with $x = 1 - 3$ and $1 \leq y \leq 2x + 2$. For the systems with $y = 2x + 2$, as well as for C_2H_4, we have observed that in the low energy region (below $\sim$ 20 keV), the cross section has an energy behavior typical for the resonant electron capture processes. The charge exchange cross sections for these systems exhibit scaling properties, the validity of which has been extended also to the collision systems with large number of H atoms in the C_xH_y molecule ($y \geq 2x - 1$). In the high energy region (above $\sim$ 100 keV), the cross sections for all systems investigated experimentally so far, also show scaling properties. These cross section scalings have been used to derive the cross sections for the systems with $y \geq 2x - 1$, which are consistent with the known values in the thermal energy region. For the non-resonant charge exchange processes, the cross sections have been derived by using the high energy scaling, the known thermal energy reaction rate coefficients and theoretical arguments based on Demkov's model and Massey relation (14).

The accuracy of the resonant cross sections for which experimental data were found available both in the low and high energy regions (CH_4, C_2H_4, C_2H_6, C_3H_8) is estimated to be within $15 - 20\%$. Based on the accuracy of the high-energy cross section scaling, all derived cross sections have an estimated accuracy of $30 - 40\%$ in

the region above $\sim$ 100 keV. In the energy region below $\sim$ 20 keV, the cross sections of derived resonant reactions ($y \geq 2x - 1$) have an estimated accuracy of about $20 - 30\%$ (based on the accuracy of the low energy scaling), while the accuracy of the cross sections for non-resonant reactions is much larger in this energy region (and in fact is undeterminated). In the energy range between $\sim$ 20 keV and $\sim$ 100 keV, the expected accuracy of all derived cross sections in the range $20 - 30\%$.

We have also calculated the rate coefficients of all considered charge exchange reaction in the temperature range 0.1 eV - 20 keV for five values of the "target" energy. The accuracy of the these rate coefficients is similar to that of the corresponding cross sections in the region E $\sim$ T.

Acknowledgements

We are indebted to Prof. T. Kusakabe for providing us with his cross section data for O^+, $C^+ + C_xH_y$ collisions prior to publication. Several discussions with Prof. M. Kimura are also greatfully acknowledged.

References

[1] Technical Basis for the ITER Final Design Report; ITER EDA Documentation Series No.16 (IAEA, Vienna, 1998).
Haasz, A. A., Stephens, J. A., Vietzke, E., et al., Atom. Plasma-Mater. Interact. Data Fusion, 7 (part A) (1998) 5.

[2] Reiter, D., May, Chr., Baelmans, M., et al., J. Nucl. Mater. 241-243 (1997) 342.

[3] Ehrhardt, A. B., Langer, W. D., Collisional Processes of Hydrocarbons in Hydrogen Plasmas, Report PPPL-2477 (1987) (Princeton Plasma Physics Laboratory).

[4] Alman, D. A., Ruzic, D. N., Brooks, J. N., Phys. Plasmas 7 (2000) 1421.

[5] Chamber, E. S., Report UCRL-14214 (1965).

[6] Koopman, D. J., J. Chem. Phys. 49 (1968) 5203.

[7] Collins, J. G., and Kebarle, P., J. Chem. Phys. 46 (1967) 1082.

[8] Toburen L. H. , Nakai Y., and Langley R. A., Phys. Rev. 171 (1968) 114.

[9] Elliot, M., J. de Physique 38 (1977) 24.

[10] Varghese S. L., Bissinger G., Joyce J. M., and Laubert R., Nucl. Instrum. Meth. 170 (1980) 269.

[11] Jones, M. L., Dougherty, B. M., Dillingham T. R., et al., Nucl. Instrum. Meth. B: 10/11 (1985) 142.

[12] Kusakabe, T., Asahina, K., Iida, A., et al., Phys. Rev. A (submitted).

[13] Kimura, M., Li Y., Hirsch G., and Buenker R. J., Phys. Rev. A 52 (1995) 1196.

[14] Kimura, M., Li, Y., Hirsch, G., and Buenker, R. J., Phys. Rev. A 54 (1996) 5019.

[15] Kusakabe, T., (private communication, 2000).

[16] Firsov, O. B., Zh. Exp. Theor. Fiz. 21 (1951) 1001 (in Russian).

[17] Smirnov, B. M., " Asymptotic Methods in Atomic Collision Theory ", (Nauka, Moscow, 1973)(in Russian).

[18] See, e.g., Gioumousis, G., Stevenson, D. P., J. Chem. Phys. 29 (1958) 294.

[19] See, e.g., Anicich, V. G., Huntress, W. T., Astrophys. J., Suppl. Ser. 62 (1986) 553.

[20] Millar, T. G., at al., Astron. Astrophys. Suppl. 121 (1997) 139.

[21] Hirschfelder, J. O., Curtis, C. F., Bird, R. B., "Molecular Theory of Gases and Liquids" (John Wiley, New York, 1967).

[22] Janev, R. K., Presnyakov, L. P., Shevelko, V. P., " Physics of Highly Charged Ions" (Springer-Verlag, Berlin, 1987).

[23] Bransden, B. H., McDowell, M. R. C., " Theory of Charge Exchange Collisions" (Clarendon Press, Oxford, 1992).

[24] Wagman, D. D., Evans, W. H., Parker, V. B., et al., " Selected Values of Chemical Thermodynamic Properties", NBS Technical Note 270-3 (January, 1968), U. S. Gov. Printing Office, Washington D. C. (1968).

[25] Rosenstock, H. M. et al., J. Phys. Chem. Ref. Data 6 (suppl. 1) (1977) 1.

[26] Janev, R. K., Langer, W. D., Evans, K., Post, D. E., " Atomic and Molecular Processes in Hydrogen-Helium Plasma ", (Springer-Verlig, Berlin, 1985).

Appendix: GRAPHS FOR RATE COEFFICIENTS FOR CHARGE EXCHARGE REACTIONS IN $H^+ + C_xH_y$ COLLISION SYSTEMS FOR DIFFERENT VALUES OF TARGET KINETIC ENERGY, E_i.

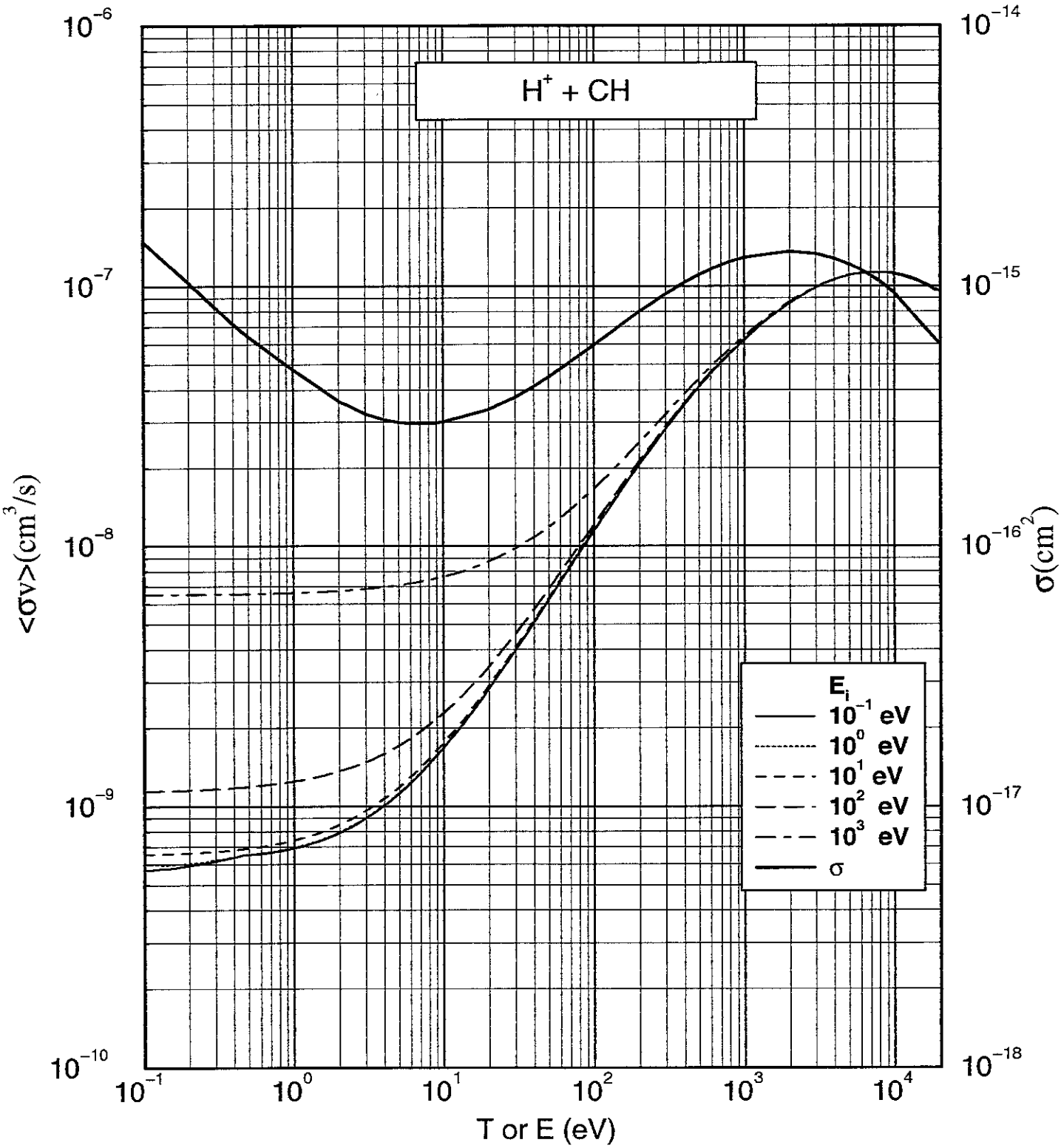
H+ + CH
10^-6
10^-7
10^-8
10^-9
10^-10
10^-14
10^-15
10^-16
10^-17
10^-18
<σv>(cm^3/s)
σ(cm^2)
10^-1
10^0
10^1
10^2
10^3
10^4
T or E (eV)
E_i
10^-1 eV
10^0 eV
10^1 eV
10^2 eV
10^3 eV
σ

Fig. 1

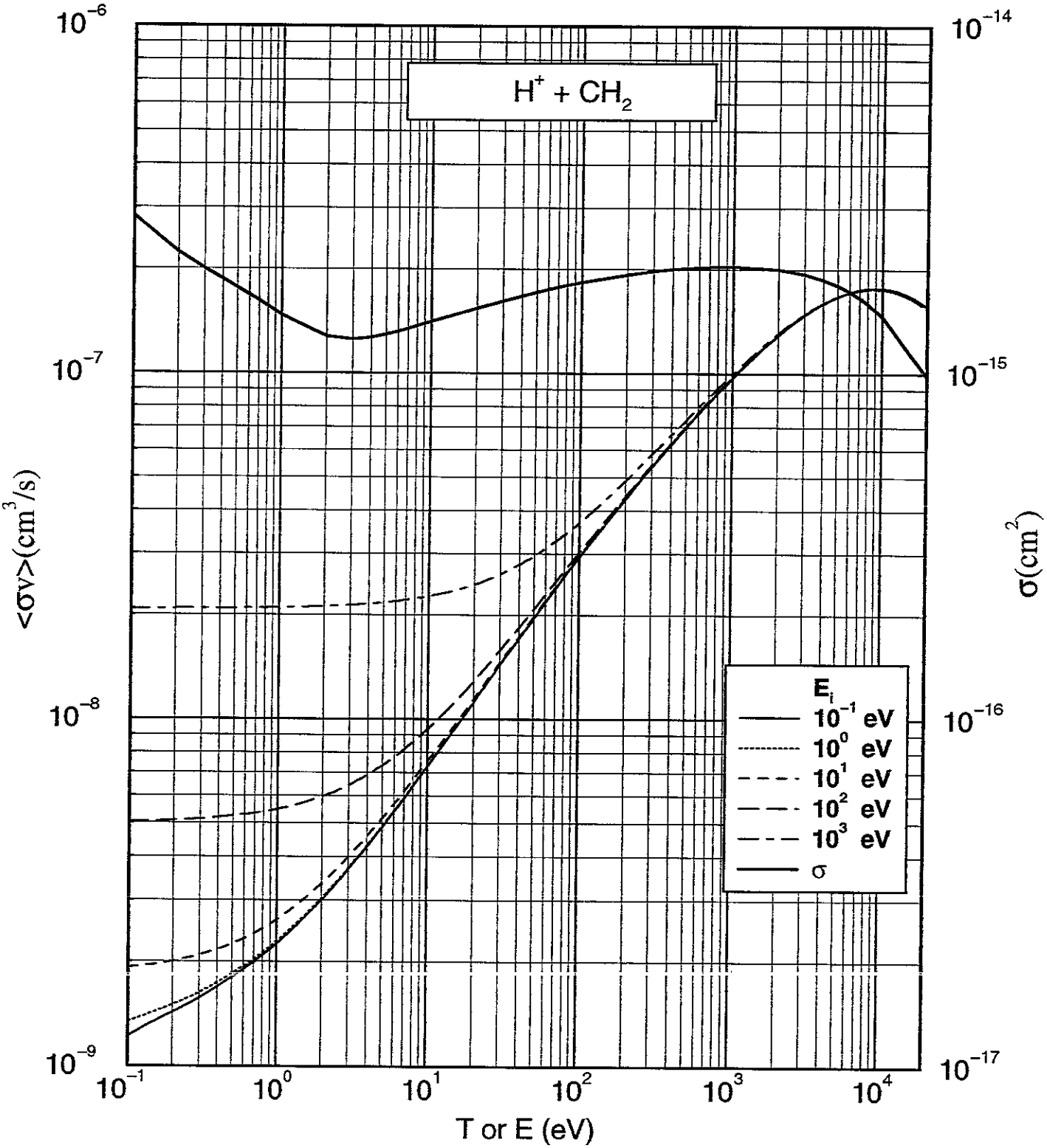
$H^+ + CH_2$
10^{-6}
10^{-7}
10^{-8}
10^{-9}
10^{-14}
10^{-15}
10^{-16}
10^{-17}
$<\sigma v>(cm^3/s)$
$\sigma(cm^2)$
10^{-1}
10^{0}
10^{1}
10^{2}
10^{3}
10^{4}
T or E (eV)
E_i
10^{-1} eV
10^{0} eV
10^{1} eV
10^{2} eV
10^{3} eV
σ

Fig. 2

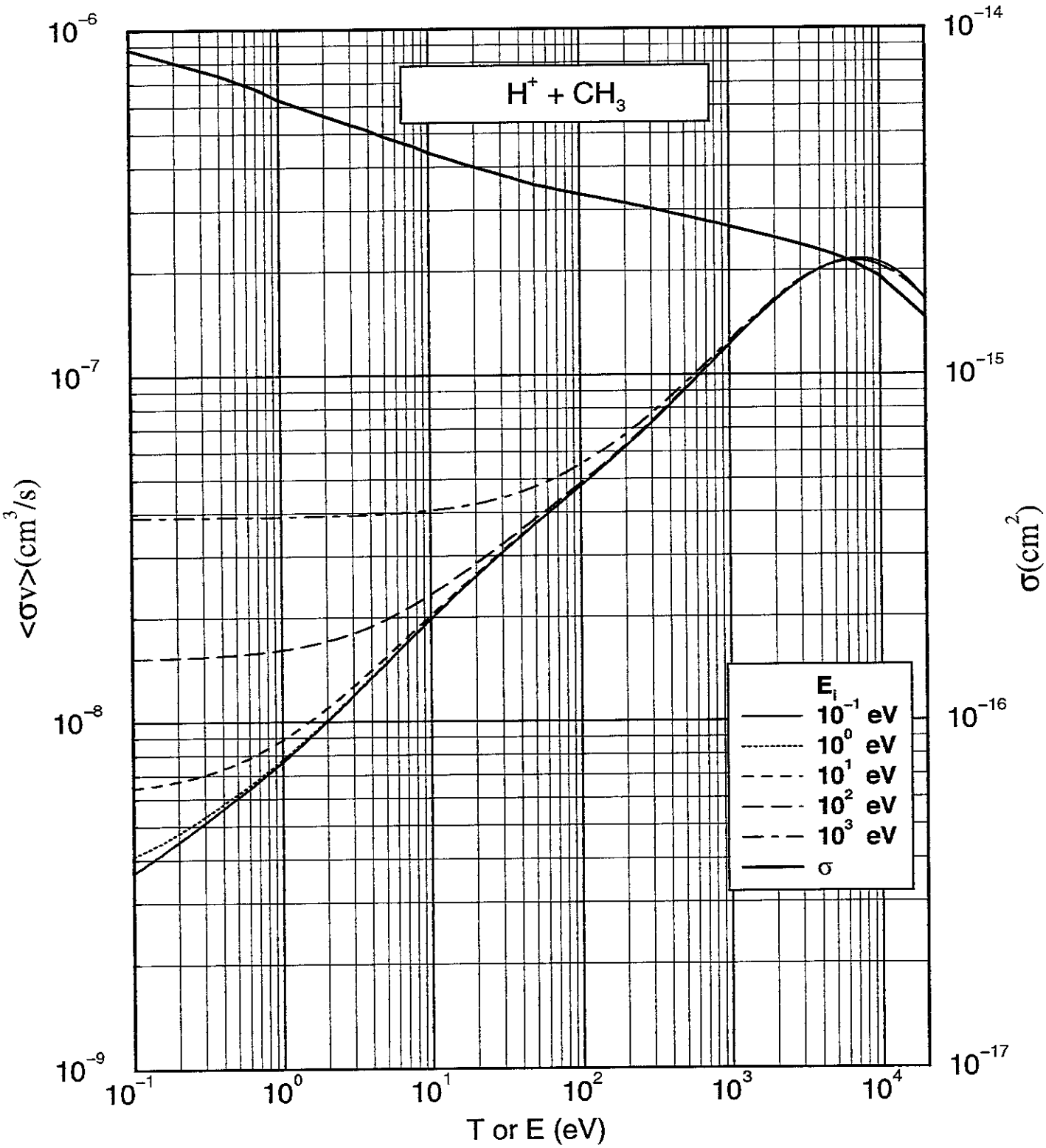
$H^+ + CH_3$
10^{-6}
10^{-7}
10^{-8}
10^{-9}
10^{-14}
10^{-15}
10^{-16}
10^{-17}
$<\sigma v>(cm^3/s)$
$\sigma(cm^2)$
10^{-1}
10^{0}
10^{1}
10^{2}
10^{3}
10^{4}
T or E (eV)
E_i
10^{-1} eV
10^{0} eV
10^{1} eV
10^{2} eV
10^{3} eV
σ

Fig. 3

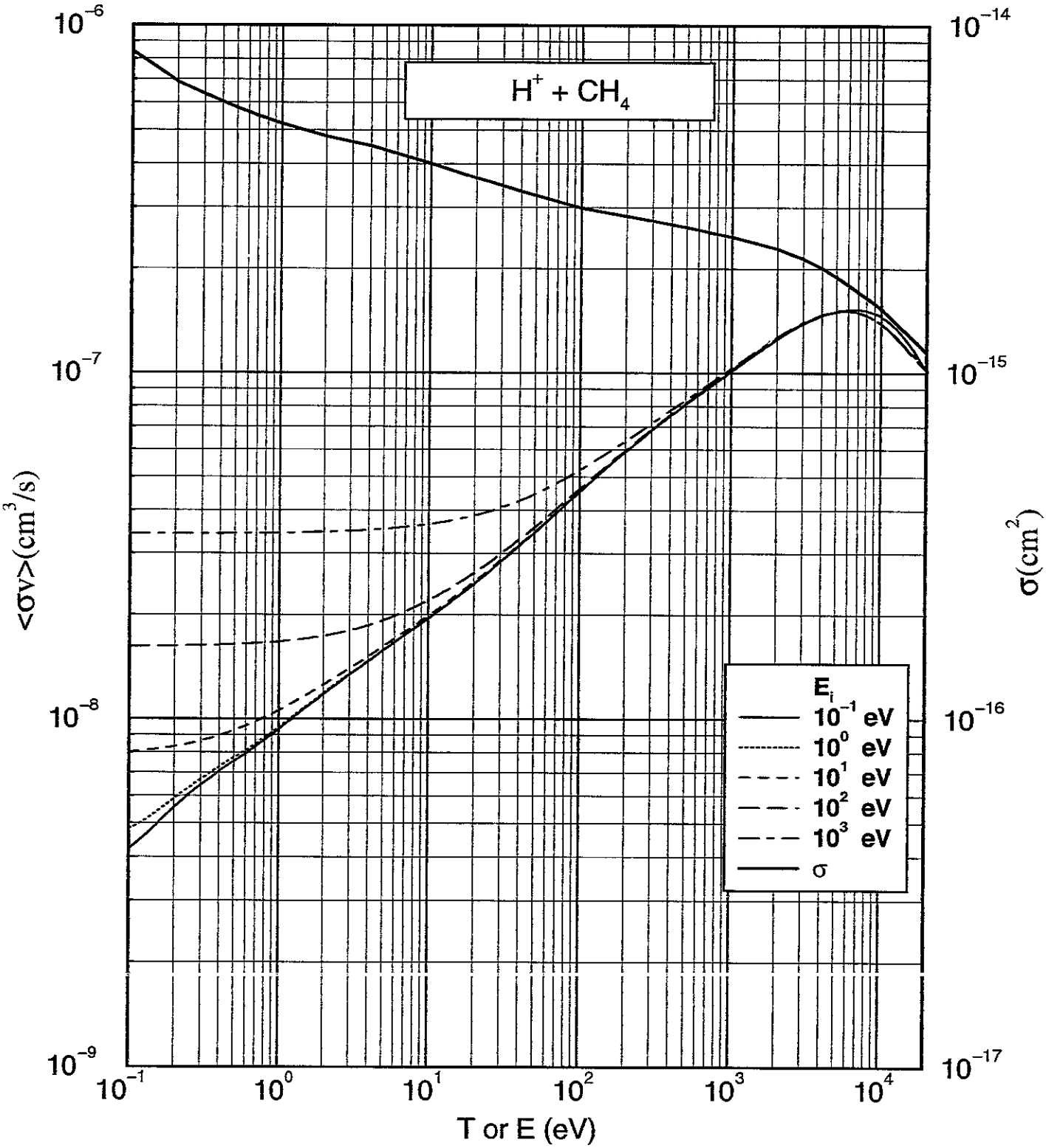
$H^+ + CH_4$
10^{-6}
10^{-7}
10^{-8}
10^{-9}
10^{-14}
10^{-15}
10^{-16}
10^{-17}
$<\sigma v>(cm^3/s)$
$\sigma(cm^2)$
10^{-1}
10^{0}
10^{1}
10^{2}
10^{3}
10^{4}
T or E (eV)
E_i
10^{-1} eV
10^{0} eV
10^{1} eV
10^{2} eV
10^{3} eV
σ

Fig. 4

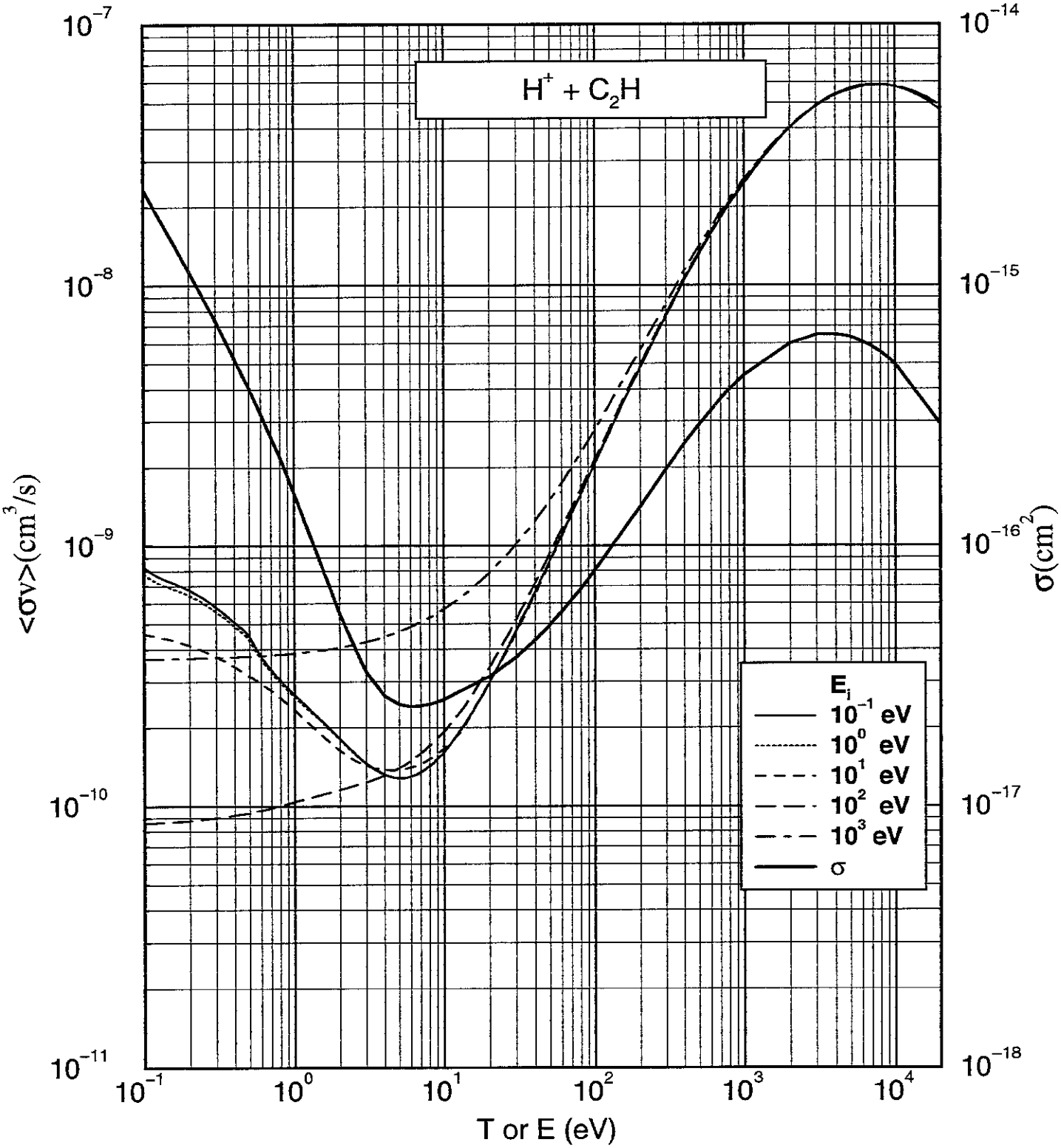
$H^+ + C_2H$
10^{-7}
10^{-8}
10^{-9}
10^{-10}
10^{-11}
$<\sigma v>(cm^3/s)$
10^{-14}
10^{-15}
10^{-16}
10^{-17}
10^{-18}
$\sigma(cm^2)$
10^{-1}
10^{0}
10^{1}
10^{2}
10^{3}
10^{4}
T or E (eV)
E_i
10^{-1} eV
10^{0} eV
10^{1} eV
10^{2} eV
10^{3} eV
σ

Fig. 5

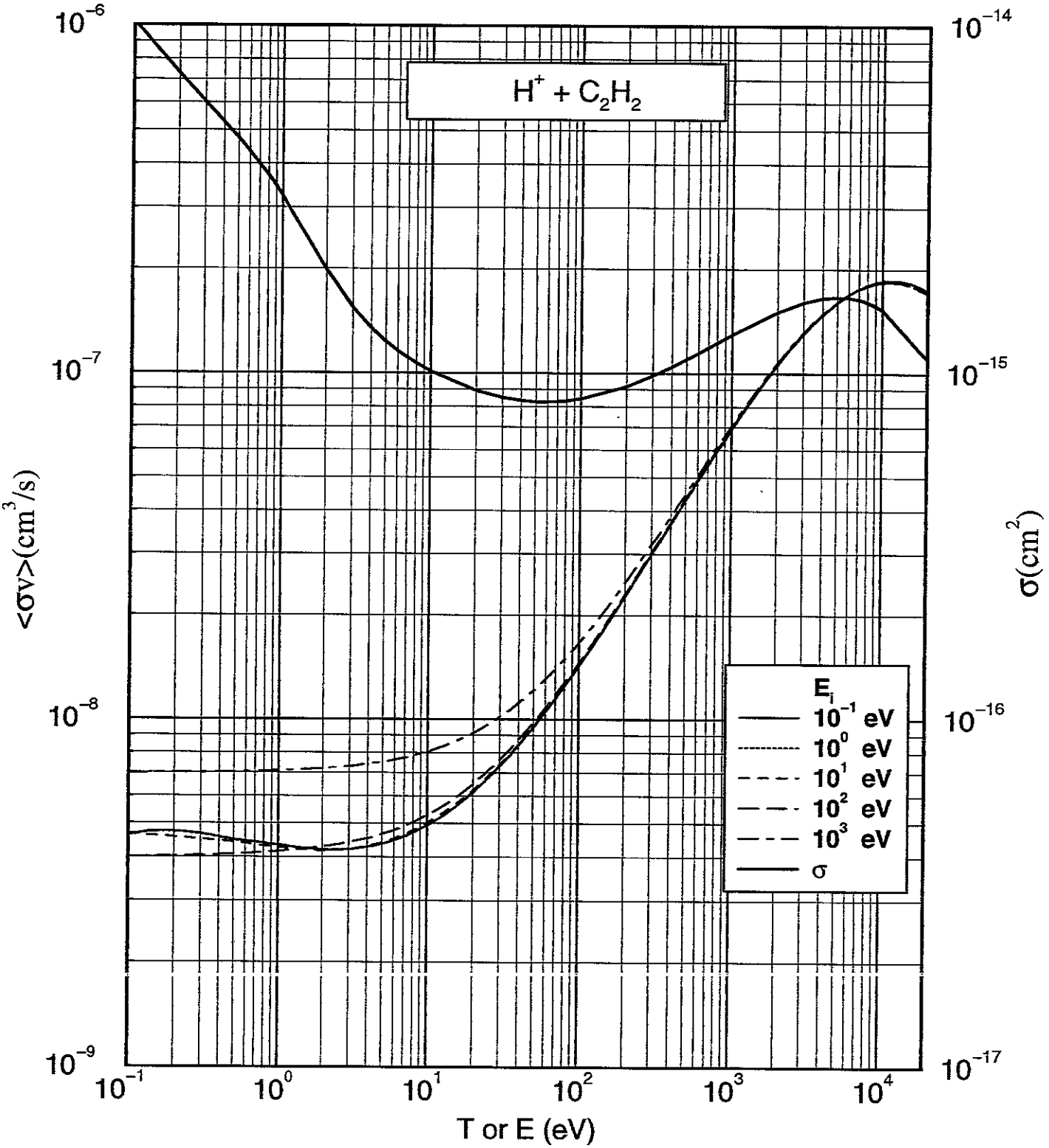
$H^+ + C_2H_2$
10^{-6}
10^{-7}
10^{-8}
10^{-9}
10^{-14}
10^{-15}
10^{-16}
10^{-17}
$<\sigma v>(cm^3/s)$
$\sigma(cm^2)$
10^{-1}
10^{0}
10^{1}
10^{2}
10^{3}
10^{4}
T or E (eV)
E_i
10^{-1} eV
10^{0} eV
10^{1} eV
10^{2} eV
10^{3} eV
σ

Fig. 6

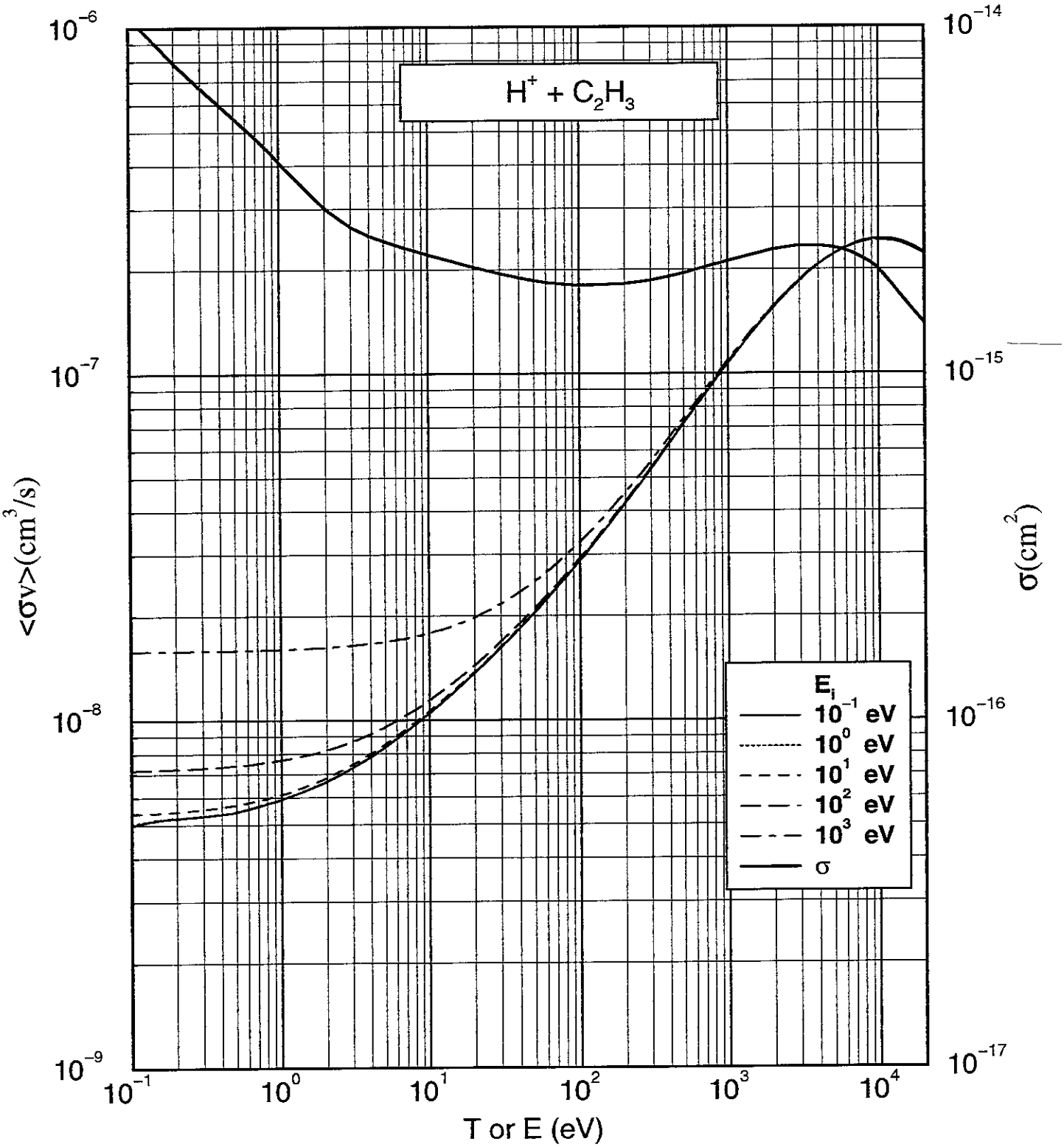
$H^+ + C_2H_3$
10^{-6}
10^{-7}
10^{-8}
10^{-9}
10^{-14}
10^{-15}
10^{-16}
10^{-17}
$<\sigma v>(cm^3/s)$
$\sigma(cm^2)$
10^{-1}
10^{0}
10^{1}
10^{2}
10^{3}
10^{4}
T or E (eV)
E_i
10^{-1} eV
10^{0} eV
10^{1} eV
10^{2} eV
10^{3} eV
σ

Fig. 7

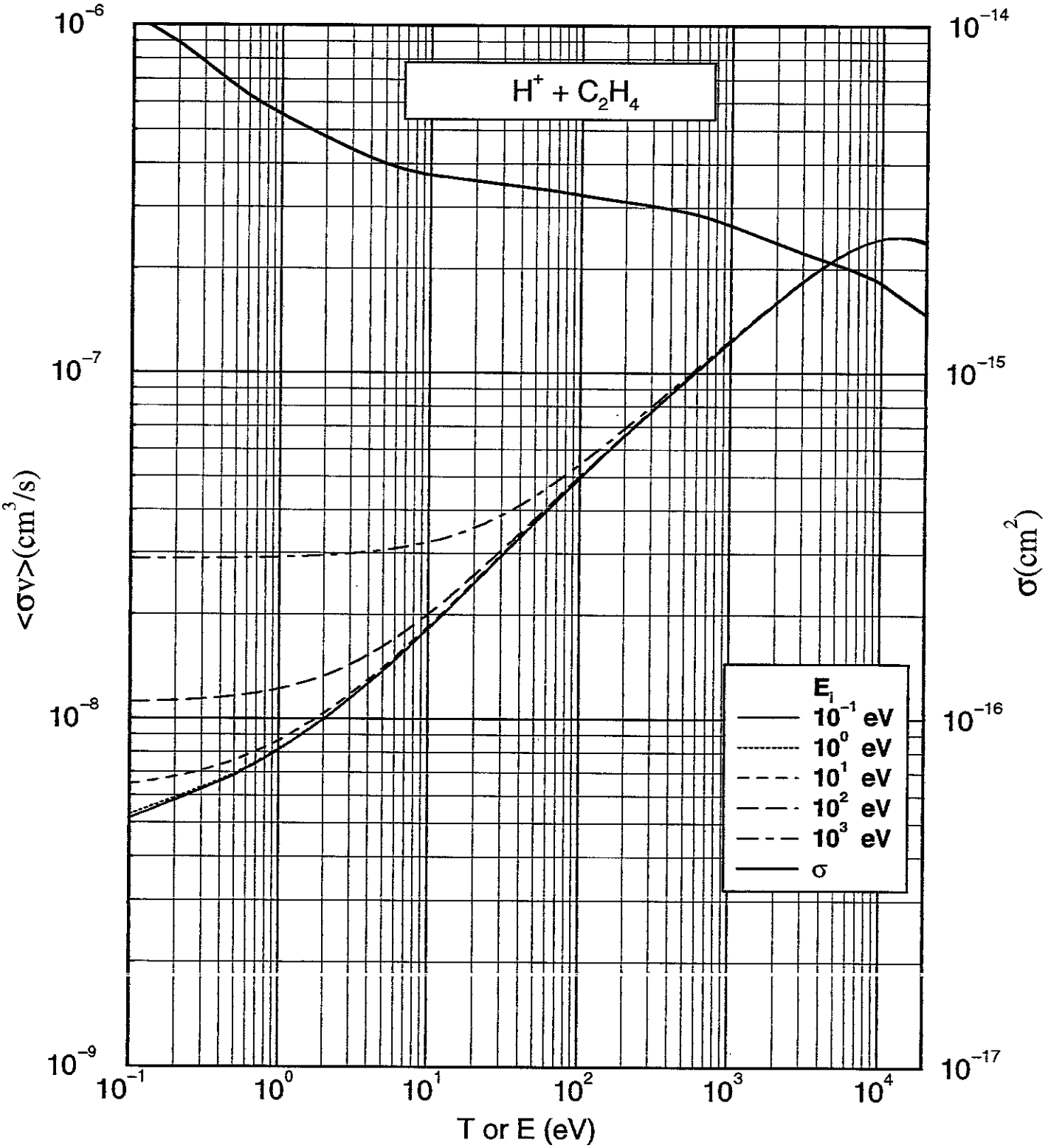
$H^+ + C_2H_4$
10^{-6}
10^{-7}
10^{-8}
10^{-9}
10^{-14}
10^{-15}
10^{-16}
10^{-17}
$<\sigma v>(cm^3/s)$
$\sigma(cm^2)$
10^{-1}
10^{0}
10^{1}
10^{2}
10^{3}
10^{4}
T or E (eV)
E_i
10^{-1} eV
10^{0} eV
10^{1} eV
10^{2} eV
10^{3} eV
σ

Fig. 8

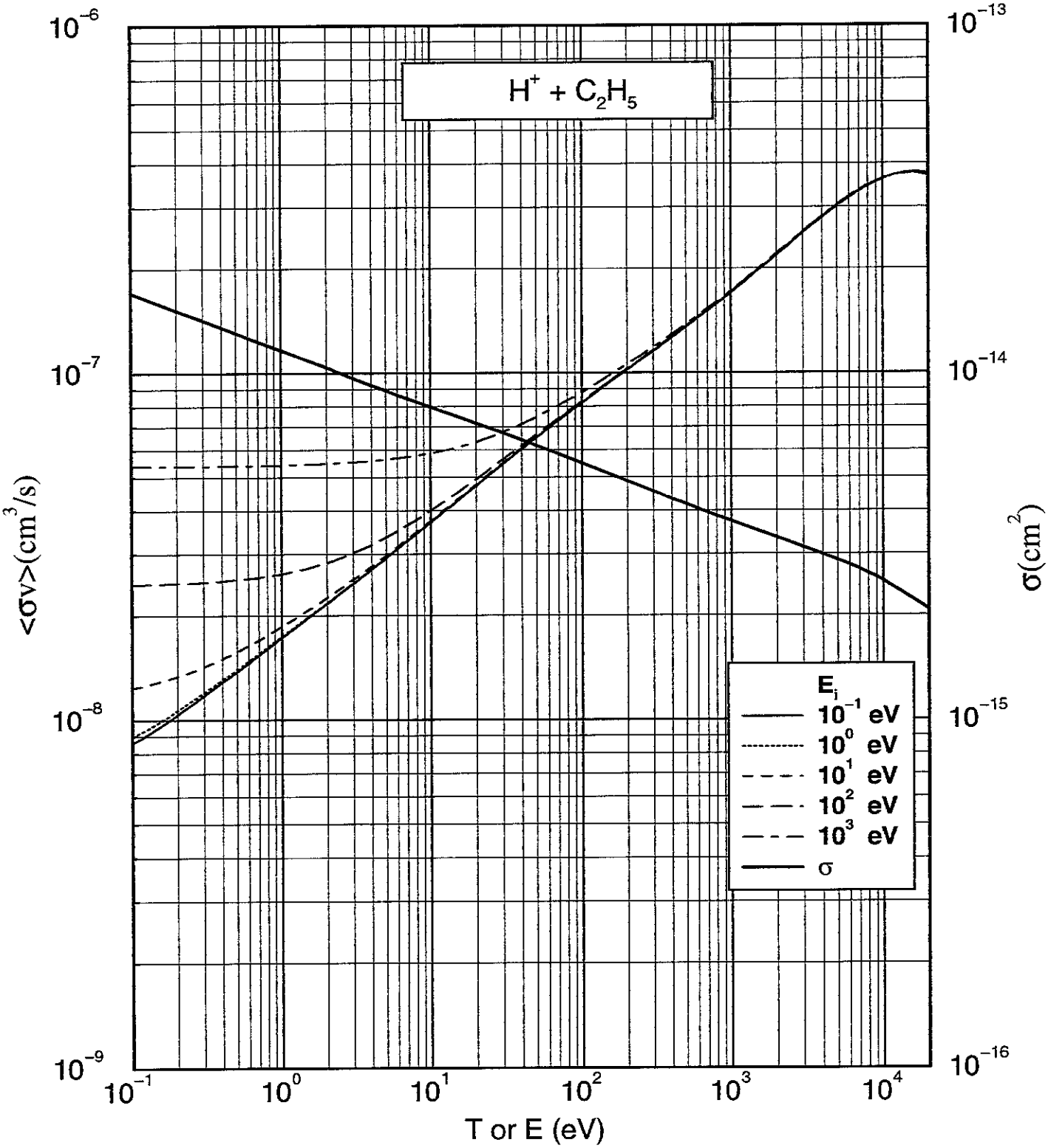
$H^+ + C_2H_5$
10^{-6}
10^{-7}
10^{-8}
10^{-9}
10^{-13}
10^{-14}
10^{-15}
10^{-16}
$<\sigma v>(cm^3/s)$
$\sigma(cm^2)$
10^{-1}
10^{0}
10^{1}
10^{2}
10^{3}
10^{4}
T or E (eV)
E_i
10^{-1} eV
10^{0} eV
10^{1} eV
10^{2} eV
10^{3} eV
σ

Fig. 9

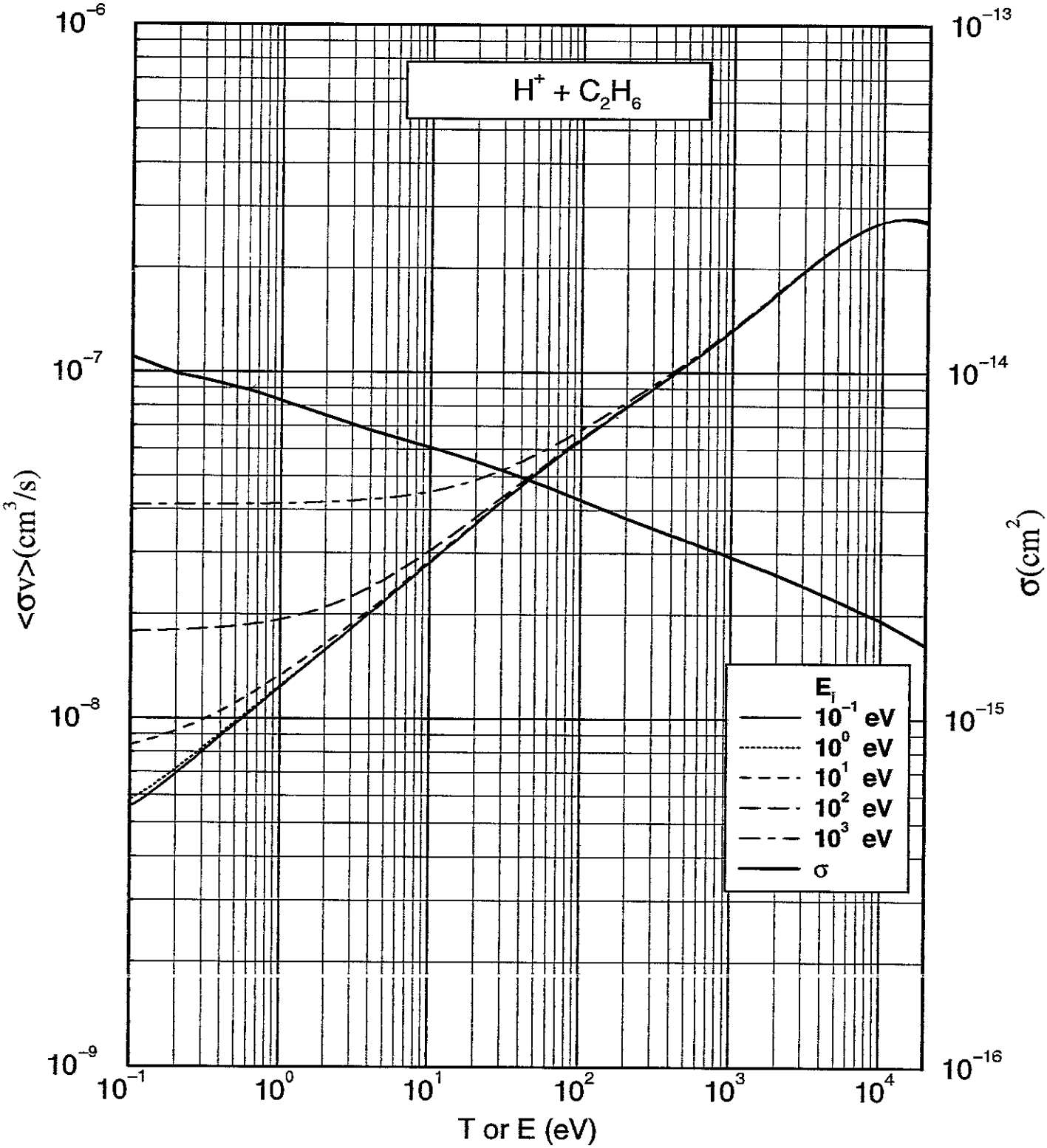
$H^+ + C_2H_6$
10^{-6}
10^{-7}
10^{-8}
10^{-9}
10^{-13}
10^{-14}
10^{-15}
10^{-16}
$<\sigma v>(cm^3/s)$
$\sigma(cm^2)$
10^{-1}
10^{0}
10^{1}
10^{2}
10^{3}
10^{4}
T or E (eV)
E_i
10^{-1} eV
10^{0} eV
10^{1} eV
10^{2} eV
10^{3} eV
σ

Fig. 10

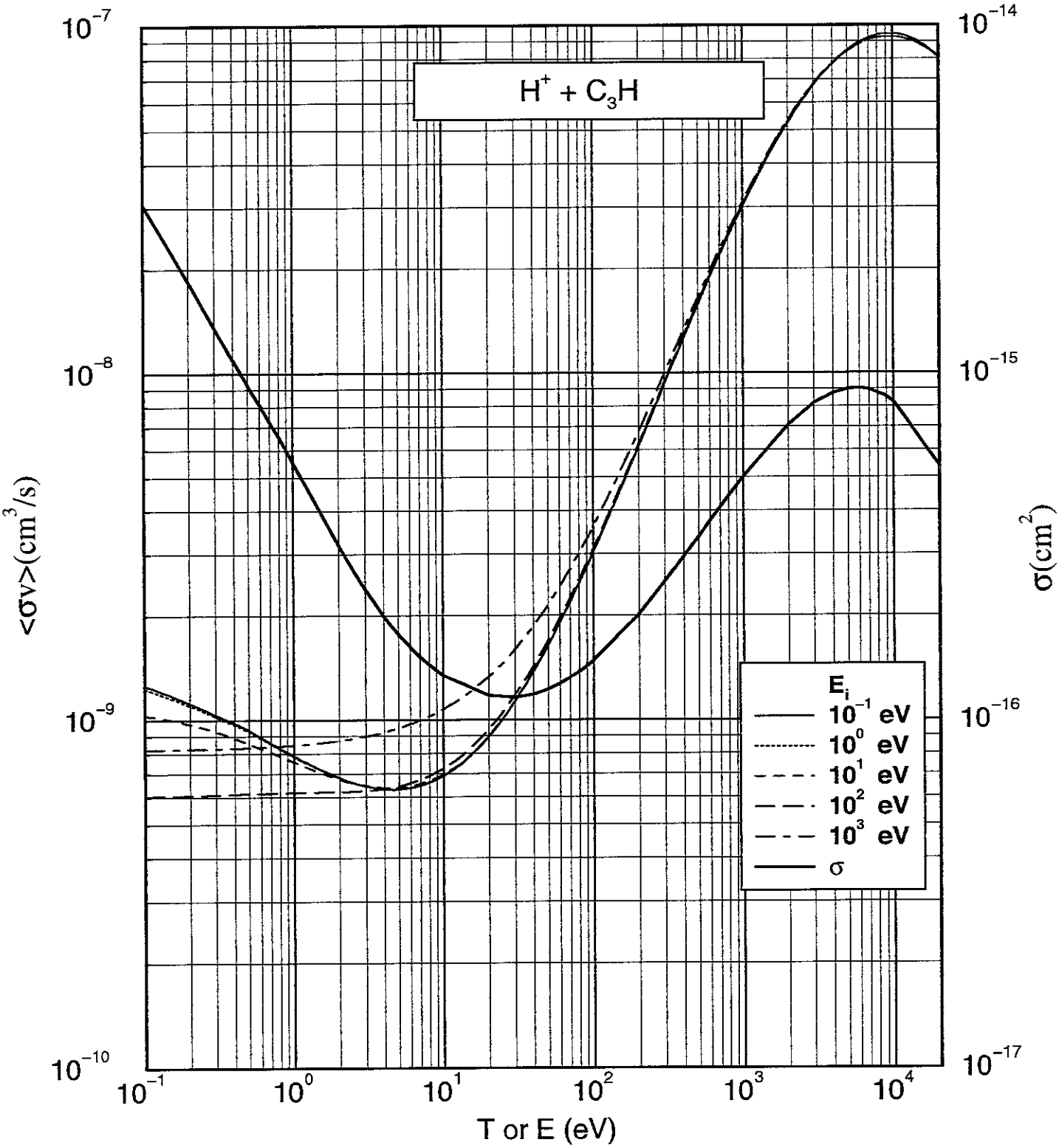
H+ + C3H
10-7
10-8
10-9
10-10
10-14
10-15
10-16
10-17
<σv>(cm3/s)
σ(cm2)
10-1
100
101
102
103
104
T or E (eV)
Ei
10-1 eV
100 eV
101 eV
102 eV
103 eV
σ

Fig. 11

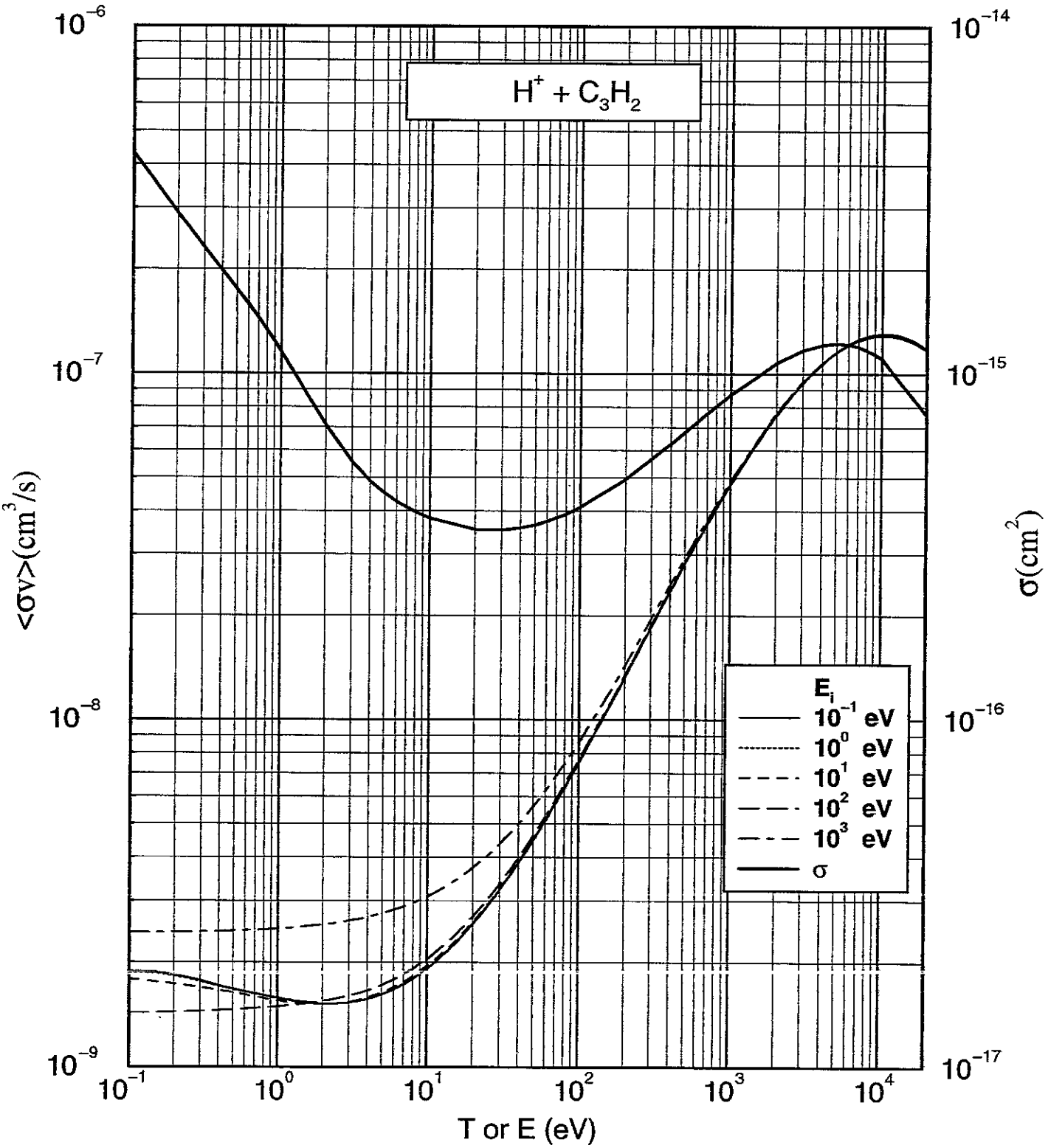
$H^+ + C_3H_2$
10^{-6}
10^{-7}
10^{-8}
10^{-9}
10^{-14}
10^{-15}
10^{-16}
10^{-17}
$<\sigma v>(cm^3/s)$
$\sigma(cm^2)$
10^{-1}
10^{0}
10^{1}
10^{2}
10^{3}
10^{4}
T or E (eV)
E_i
10^{-1} eV
10^{0} eV
10^{1} eV
10^{2} eV
10^{3} eV
σ

Fig. 12

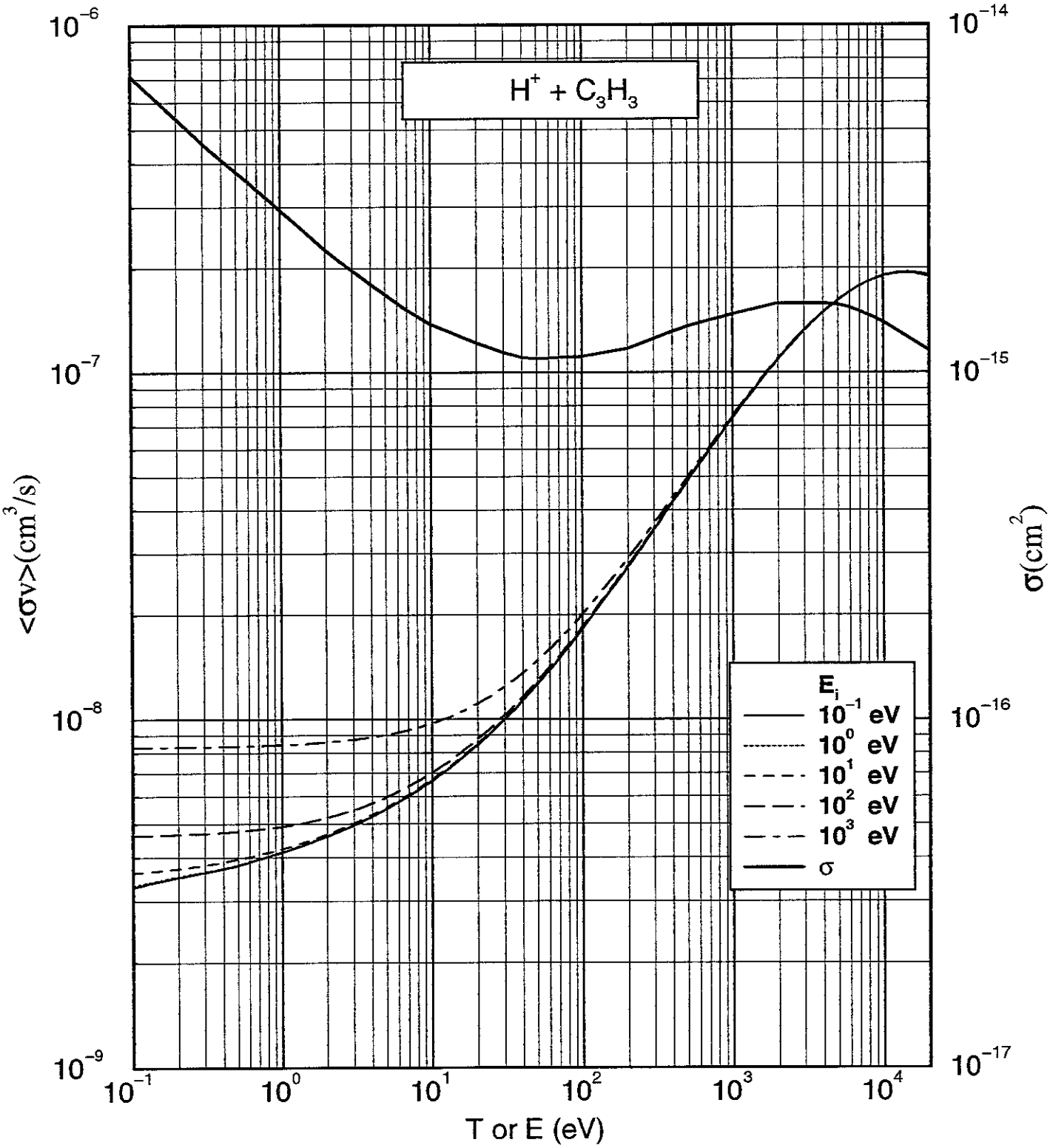
$H^+ + C_3H_3$
10^{-6}
10^{-7}
10^{-8}
10^{-9}
10^{-14}
10^{-15}
10^{-16}
10^{-17}
$<\sigma v>(cm^3/s)$
$\sigma(cm^2)$
10^{-1}
10^{0}
10^{1}
10^{2}
10^{3}
10^{4}
T or E (eV)
E_i
10^{-1} eV
10^{0} eV
10^{1} eV
10^{2} eV
10^{3} eV
σ

Fig. 13

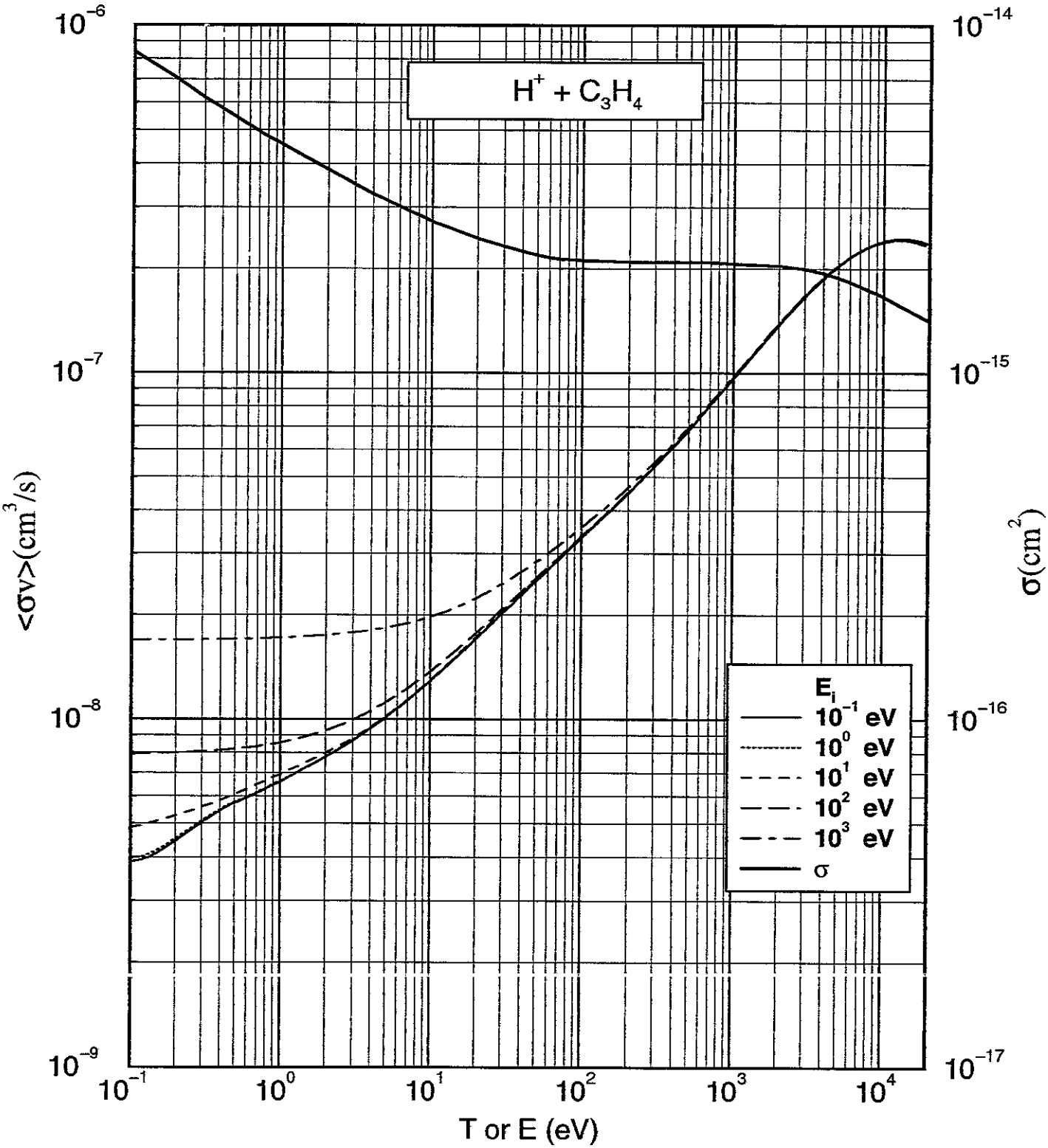
$H^+ + C_3H_4$
10^{-6}
10^{-7}
10^{-8}
10^{-9}
10^{-14}
10^{-15}
10^{-16}
10^{-17}
$<\sigma v>(cm^3/s)$
$\sigma(cm^2)$
10^{-1}
10^{0}
10^{1}
10^{2}
10^{3}
10^{4}
T or E (eV)
E_i
10^{-1} eV
10^{0} eV
10^{1} eV
10^{2} eV
10^{3} eV
σ

Fig. 14

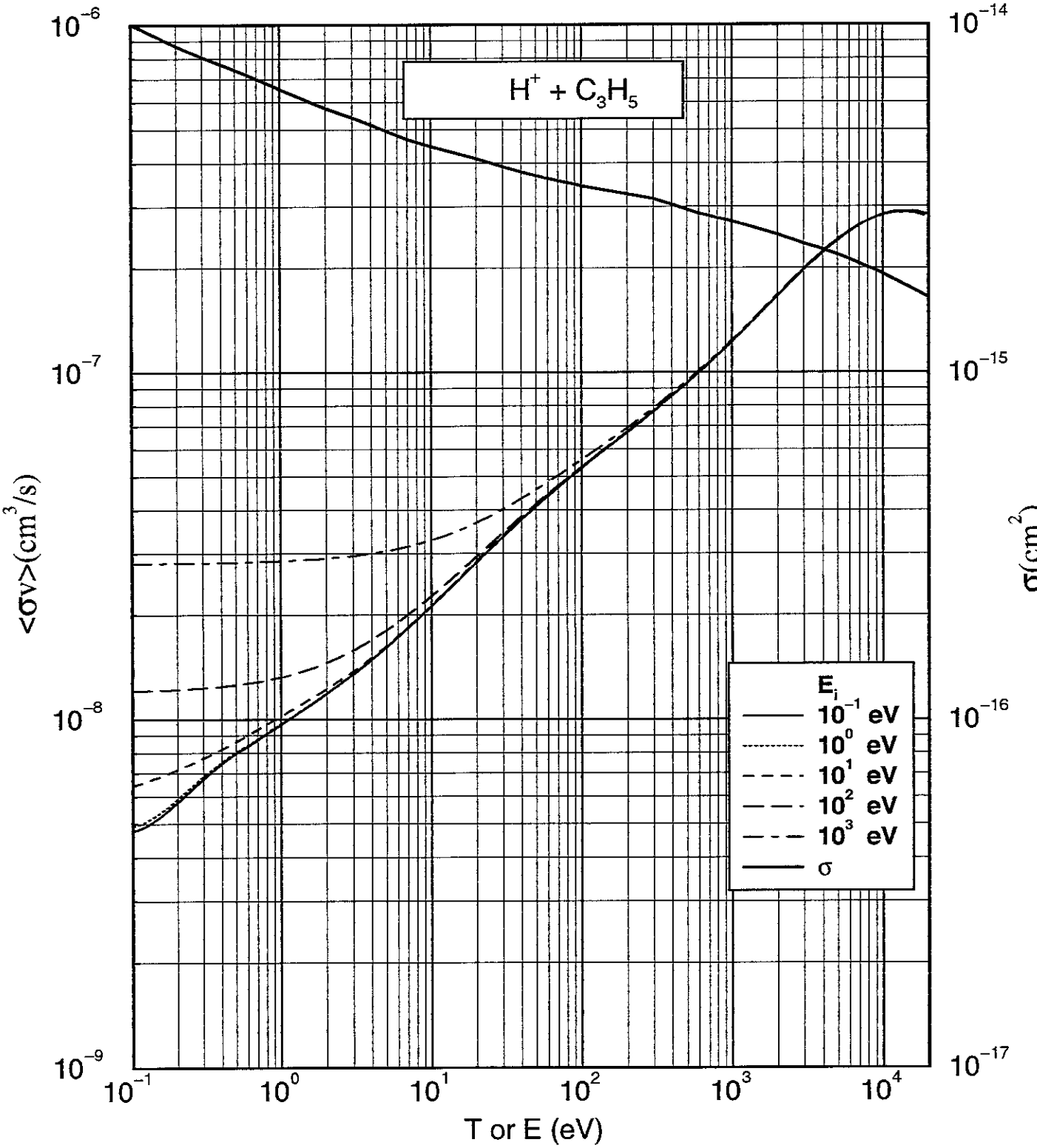
$H^+ + C_3H_5$
10^{-6}
10^{-7}
10^{-8}
10^{-9}
10^{-14}
10^{-15}
10^{-16}
10^{-17}
$<\sigma v>(cm^3/s)$
$\sigma(cm^2)$
10^{-1}
10^{0}
10^{1}
10^{2}
10^{3}
10^{4}
T or E (eV)
E_i
10^{-1} eV
10^{0} eV
10^{1} eV
10^{2} eV
10^{3} eV
σ

Fig. 15

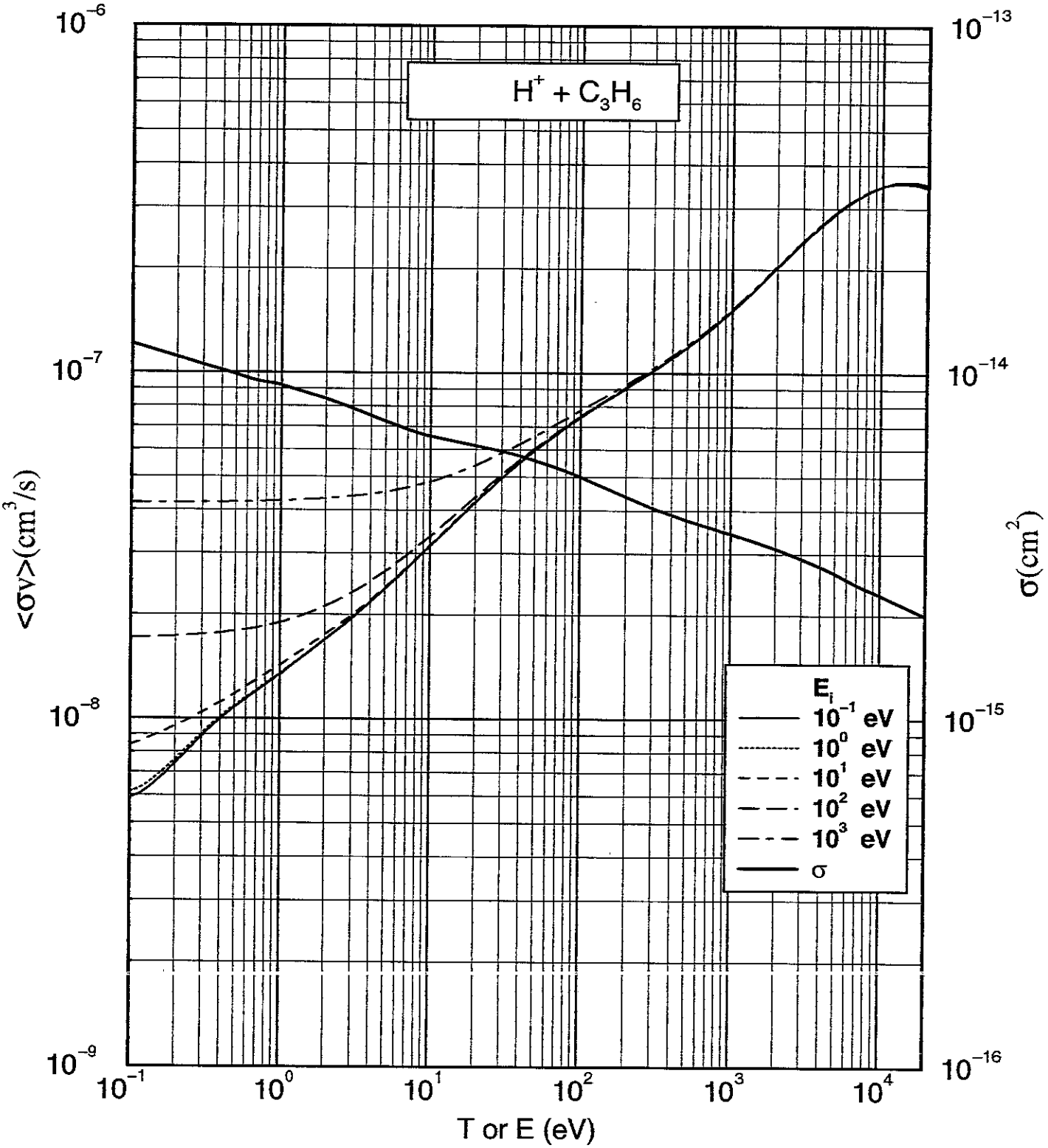
$H^+ + C_3H_6$
10^{-6}
10^{-7}
10^{-8}
10^{-9}
10^{-13}
10^{-14}
10^{-15}
10^{-16}
$<\sigma v>(cm^3/s)$
$\sigma(cm^2)$
10^{-1}
10^{0}
10^{1}
10^{2}
10^{3}
10^{4}
T or E (eV)
E_i
10^{-1} eV
10^{0} eV
10^{1} eV
10^{2} eV
10^{3} eV
σ

Fig. 16

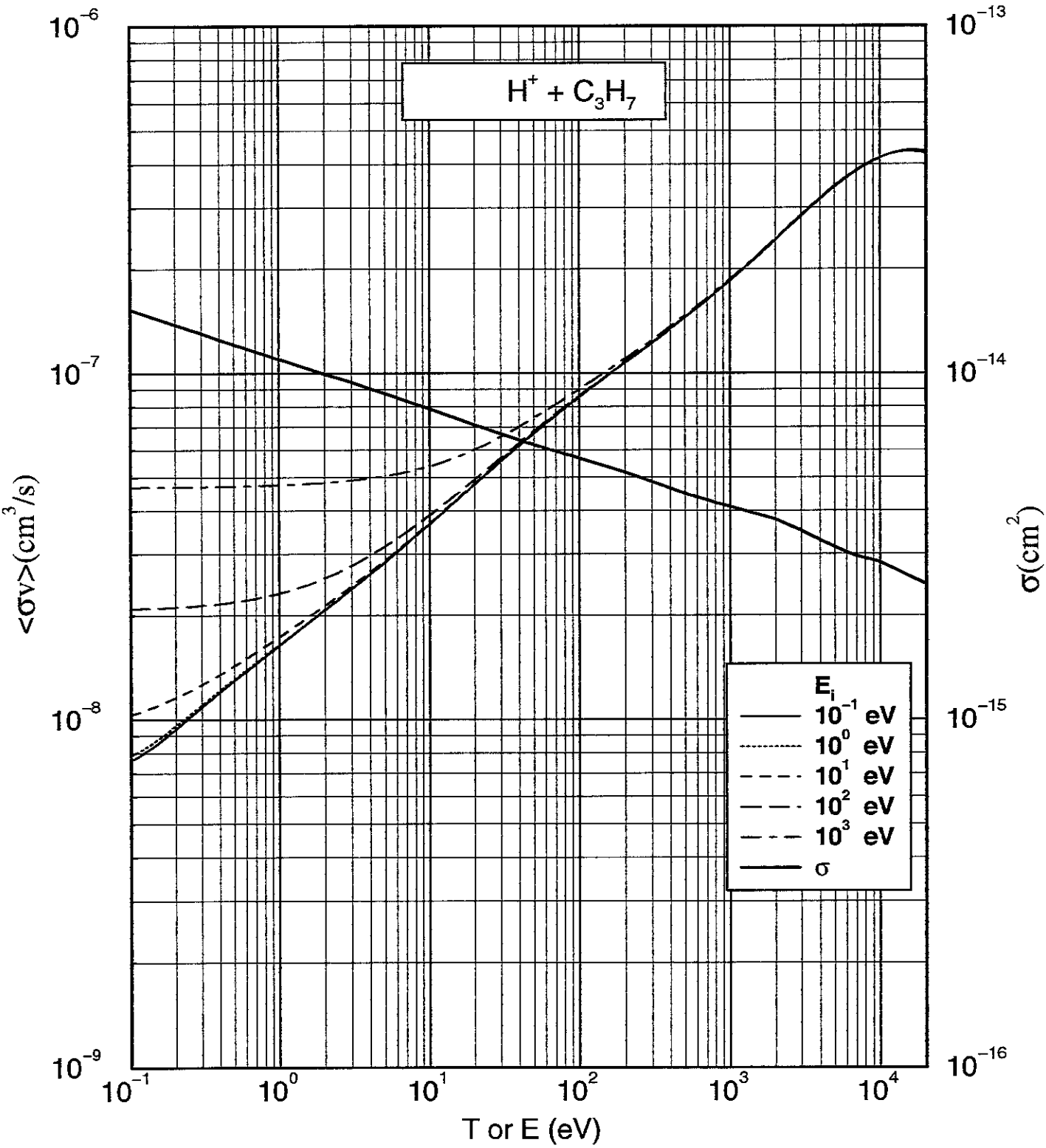
$H^+ + C_3H_7$
10^{-6}
10^{-7}
10^{-8}
10^{-9}
10^{-13}
10^{-14}
10^{-15}
10^{-16}
$<\sigma v>(cm^3/s)$
$\sigma(cm^2)$
10^{-1}
10^{0}
10^{1}
10^{2}
10^{3}
10^{4}
T or E (eV)
E_i
10^{-1} eV
10^{0} eV
10^{1} eV
10^{2} eV
10^{3} eV
σ

Fig. 17

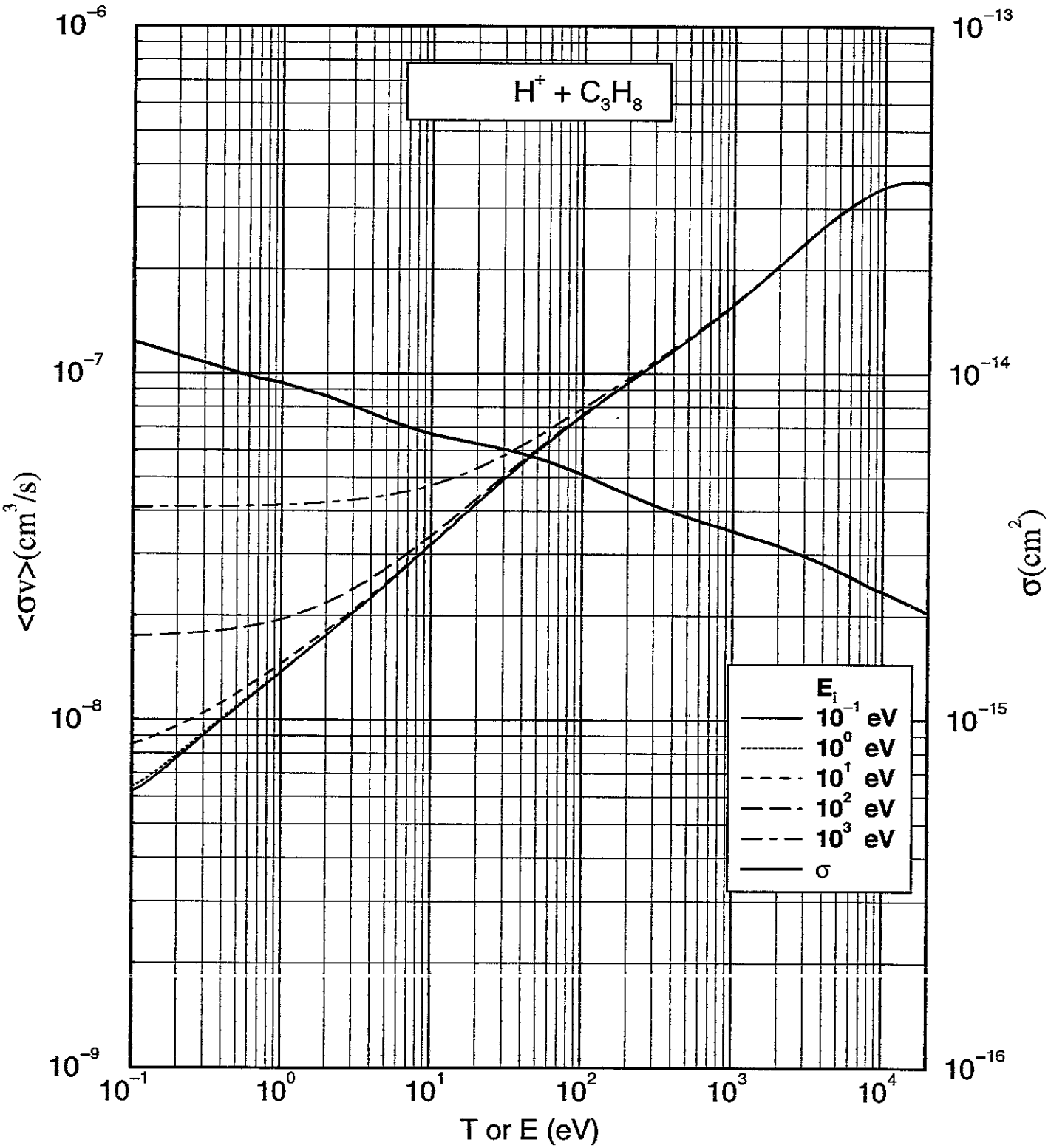
$H^+ + C_3H_8$
10^{-6}
10^{-7}
10^{-8}
10^{-9}
10^{-13}
10^{-14}
10^{-15}
10^{-16}
$<\sigma v>(cm^3/s)$
$\sigma(cm^2)$
10^{-1}
10^{0}
10^{1}
10^{2}
10^{3}
10^{4}
T or E (eV)
E_i
10^{-1} eV
10^{0} eV
10^{1} eV
10^{2} eV
10^{3} eV
σ

Fig. 18

Recent Issues of NIFS-DATA Series

NIFS-DATA-42 H Tawara,
Bibliography on Electron Transfer Processes in Ion-ion / Atom / Molecule Collisions -Updated 1997 -,
May 1997

NIFS-DATA-43 M Goto and T Fujimoto,
Collisional-radiative Model for Neutral Helium in Plasma· Excitation Cross Section and Singlet-triplet Wavefunction Mixing, Oct 1997

NIFS-DATA-44 J. Dubau, T Kato and U.I Safronova,
Dielectronic Recombination Rate Coefficients to the Excited States of Cl From ClI, Jan 1998

NIFS-DATA-45 Y. Yamamura, W. Takeuchi and T. Kawamura,
The Screening Length of Interatomic Potential in Atomic Collisions; Mar 1998

NIFS-DATA-46 T Kenmotsu, T Kawamura, T Ono and Y Yamamura,
Dynamical Simulation for Sputtering of B4C; Mar 1998

NIFS-DATA-47 I. Murakami, K Moribayashi and T Kato,
Effect of Recombination Processes on FeXXIII Line Intensities, May 1998

NIFS-DATA-48 Zhijie Li, T Kenmotsu, T Kawamura, T Ono and Y Yamamura,
Sputtering Yield Calculations Using an Interatomic Potential with the Shell Effect and a New Local Model, Oct 1998

NIFS-DATA-49 S Sasaki, M Goto, T Kato and S. Takamura,
Line Intensity Ratios of Helium Atom in an Ionizing Plasma, Oct 1998

NIFS-DATA-50 I. Murakami, T Kato and U Safronova,
Spectral Line Intensities of NeVII for Non-equilibrium Ionization Plasma Including Dielectronic Recombination Processses, Jan 1999

NIFS-DATA-51 Hiro Tawara and Masa Kato,
Electron Impact Ionization Data for Atoms and Ions -up-dated in 1998-; Feb 1999

NIFS-DATA-52 J G. Wang, T Kato and I. Murakami,
Validity of n^{-3} Scaling Law in Dielectronic Recombination Processes; Apr. 1999

NIFS-DATA-53 J G. Wang, T Kato and I Murakami,
Dielectronic Recombination Rate Coefficients to Excited States of He from He^{+}, Apr 1999

NIFS-DATA-54 T Kato and E. Asano,
Comparison of Recombination Rate Coefficients Given by Empirical Formulas for Ions from Hydrogen through Nickel; June 1999

NIFS-DATA-55 H P Summers, H. Anderson, T Kato and S Murakami,
Hydrogen Beam Stopping and Beam Emission Data for LHD; Nov 1999

NIFS-DATA-56 S Born, N. Matsunami and H. Tawara,
A Simple Theoretical Approach to Determine Relative Ion Yield (RIY) in Glow Discharge Mass Spectrometry (GDMS); Jan 2000

NIFS-DATA-57 T Ono, T Kawamura, T Kenmotsu, Y. Yamamura,
Simulation Study on Retention and Reflection from Tungsten Carbide under High Fluence of Helium Ions, Aug 2000

NIFS-DATA-58 J.G. Wang, M Kato and T Kato,
Spectra of Neutral Carbon for Plasma Diagnostics; Oct 2000

NIFS-DATA-59 Yu. V. Ralchenko, R. K. Janev, T Kato, D V Fursa, I. Bray and F J de Heer
Cross Section Database for Collision Processes of Helium Atom with Charged Particles
I. Electron Impact Processes; Oct. 2000

NIFS-DATA-60 U.I Safronova, C. Namba, W R. Johnson, M S. Safronova,
Relativistic Many-Body Calculations of Energies for n = 3 States in Aluminiumlike Ions, Jan 2001

NIFS-DATA-61 U.I Safronova, C. Namba, I Murakami, W.R. Johnson and M S Safronova,
E1,E2, M1, and M2 Transitions in the Neon Isoelectronic Sequence, Jan. 2001

NIFS-DATA-62 R K. Janev, Yu.V Ralchenko, T Kenmotsu,
Unified Analytic Formula for Physical Sputtering Yield at Normal Ion Incidence; Apr. 2001

NIFS-DATA-63 Y Itikawa,
Bibliography on Electron Collisions with Molecules. Rotational and Vibrational Excitations, 1980-2000 Apr 2001

NIFS-DATA-64 R K. Janev, J G. Wang and T.Kato,
Cross Sections and Rate Coefficients for Charge Exchange Reactions of Protons with Hydrocarbon Molecules, May 2001